Journal of Instrumentation

Reconstruction of signal amplitudes in the CMS electromagnetic calorimeter in the presence of overlapping proton-proton interactions

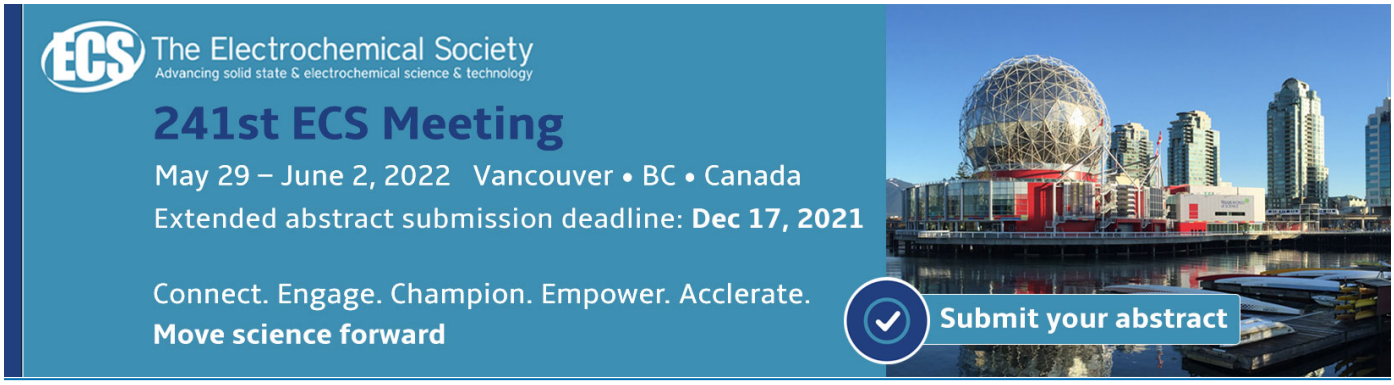

Published by IOP Publishing for Sissa Medialab

Received: *June 25, 2020*
Accepted: *August 15, 2020*
Published: *October 1, 2020*

Reconstruction of signal amplitudes in the CMS electromagnetic calorimeter in the presence of overlapping proton-proton interactions

The CMS collaboration

E-mail: cms-publication-committee-chair@cern.ch

Abstract: A template fitting technique for reconstructing the amplitude of signals produced by the lead tungstate crystals of the CMS electromagnetic calorimeter is described. This novel approach is designed to suppress the contribution to the signal of the increased number of out-of-time interactions per beam crossing following the reduction of the accelerator bunch spacing from 50 to 25 ns at the start of Run 2 of the LHC. Execution of the algorithm is sufficiently fast for it to be employed in the CMS high-level trigger. It is also used in the offline event reconstruction. Results obtained from simulations and from Run 2 collision data (2015–2018) demonstrate a substantial improvement in the energy resolution of the calorimeter over a range of energies extending from a few GeV to several tens of GeV.

Keywords: Large detector-systems performance; Pattern recognition, cluster finding, calibration and fitting methods

ArXiv ePrint: 2006.14359

https://doi.org/10.1088/1748-0221/15/10/P10002

2020 JINST 15 P10002

Contents

2020 JINST 15 P10002

1 Introduction

The central feature of the CMS apparatus is a superconducting solenoid of 6 m internal diameter, providing a magnetic field of 3.8 T. Within the solenoid volume are a silicon pixel and strip tracker, a lead tungstate ($PbWO_4$) crystal electromagnetic calorimeter (ECAL), which is the focus of this paper, and a brass and scintillator hadron calorimeter (HCAL), each composed of a barrel and two endcap sections. Forward calorimeters extend the pseudorapidity coverage provided by the barrel and endcap detectors. Muons are detected in gas-ionization chambers embedded in the steel flux-return yoke outside the solenoid. A more detailed description of the CMS detector is given in ref. [1].

The ECAL consists of 61 200 $PbWO_4$ crystals mounted in the barrel section (EB), covering the range of pseudorapidity $|\eta| < 1.48$, closed by 7324 crystals in each of the two endcaps (EE), covering the range $1.48 < |\eta| < 3.0$. The EB uses 23 cm long crystals with front-face cross sections of approximately $2.2\times2.2\,cm^2$, while the EE contains 22 cm long crystals with a front-face cross section of $2.86\times2.86\,cm^2$. The scintillation light is detected by avalanche photodiodes (APDs) in the EB and by vacuum phototriodes (VPTs) in the EE. The $PbWO_4$ crystals have a Molière radius of 2.19 cm, approximately matching the transverse dimensions of the crystals. A preshower detector consisting of two planes of silicon sensors interleaved with lead for a total of 3 radiation lengths is located in front of EE [2]. A crystal transparency monitoring system, based on the injection of laser light at 447 nm, close to the emission peak of scintillation light from $PbWO_4$, is used to track and correct for response changes during LHC operation [3, 4].

The LHC operating conditions during Run 2 data taking (2015–2018) were more challenging than those of Run 1 (2010–2013) in several respects. The center-of-mass energy of the collisions was raised from 8 to 13 TeV, the bunch spacing (the time interval between neighboring bunches), was halved from 50 ns to the design value of 25 ns, and the instantaneous luminosity reached $2.1\times10^{34}\,cm^{-2}\,s^{-1}$ compared to $0.75\times10^{34}\,cm^{-2}\,s^{-1}$ achieved in 2012.

The mean number of additional interactions in a single bunch crossing (BX), termed pileup (PU), in Run 2 was 34, with the tail of the distribution extending up to 80. The average values for 2016, 2017 and 2018 were 27, 38 and 37, respectively. For the results shown in this paper, obtained from simulations, an average number of 40 interactions per bunch crossing is used. For comparison, during Run 1 in 2012, the mean value was 21 interactions per BX, with an extreme value of 40. After shaping by the electronics, the ECAL signals extend over several hundred nanoseconds. Consequently, the decrease in the LHC bunch spacing from 50 to 25 ns results in an increased number of overlapping signals from neighboring BXs, referred to as out-of-time (OOT) pileup. These spurious signals effectively add to the electronic noise and degrade the energy resolution of the calorimeter. To reduce these effects, an innovative ECAL amplitude reconstruction procedure, based on a template fitting technique, named "multifit", was introduced in 2015, before the start of Run 2. The new algorithm replaces the one used during Run 1 ("weights" method) [5], which was based on a digital-filtering technique. The original algorithm performed well under the conditions of Run 1, but was not suitable for Run 2 because of the increased OOT pileup.

2 Data and simulated samples

The results shown in this paper are based on subsets of the data samples recorded by the CMS experiment in proton-proton (pp) collisions at a center-of-mass energy of 13 TeV. Calibration samples are recorded by using special data streams, based either on a minimal single-crystal energy deposit, or on diphoton invariant mass, to profit from the copious production of π^0 mesons subsequently decaying into $\gamma\gamma$. Performances are evaluated on a subset of the standard physics stream of the high-level trigger (HLT), by using electrons from Z-boson decays ($Z \to e^+e^-$).

In addition to data samples from calibration sources and collision data, two kinds of Monte Carlo (MC) samples are used. One is the full detector simulation used for physics analyses, implemented with GEANT4 [6], of single photons within the CMS detector with a uniform distribution in η and a flat transverse momentum p_T spectrum extending from 1 to 100 GeV. These events are generated

2020 JINST 15 P10002

with the PYTHIA 8.226 [7] package and its CUETP8M1 [8] tune for parton showering, hadronization, and underlying event simulation. These events are used to study the performance of the algorithm when the showering of an electromagnetic particle spreads across more than a single crystal, which is typical of most energy deposits in the ECAL. The second set of MC samples is produced by a fast stand-alone simulation, where the single-crystal amplitudes are generated by pseudo-experiments using a parametric representation of the pulse shape and the measured covariance matrix. Energy deposits typical of the PU present in Run 2 are then added to these signals. Additional pp interactions in the same or adjacent BXs are added to each simulated event sample, with an average number of 40.

3 The electromagnetic calorimeter readout

The electrical signal from the photodetectors is amplified and shaped using a multigain preamplifier (MGPA), which provides three simultaneous analogue outputs that are shaped to have a rise time of approximately 50 ns and fall to 10% of the peak value in 400 ns [2]. The shaped signals are sampled at the LHC bunch-crossing frequency of 40 MHz and digitized by a system of three channels of floating-point Analog-to-Digital Converters (ADCs). The channel with the gain that gives the highest nonsaturated value is selected sample-by-sample, thus providing a dynamic range from 35 MeV to 1.7 TeV in the barrel. A time frame of 10 consecutive samples is read out every 25 ns, in synchronization with the triggered LHC BX [2]. The convention used throughout this report is to number samples starting from 0. The phase of the readout is adjusted such that the time of the in-time pulse maximum value coincides with the fifth digitized sample. The first three samples are read out before the signal pulse rises significantly from the pedestal baseline (presamples). The 50 ns rise time of the signal pulse after amplification results from the convolution of the 10 ns decay time of the crystal scintillation emission and the 40 ns shaping time of the MGPA [1, 2, 5].

4 The multifit method

4.1 The Run 1 amplitude reconstruction of ECAL signals

During LHC Run 1, a weighting algorithm [5] was used to estimate the ECAL signal amplitudes, both online in the HLT [9] and in the offline reconstruction. With that algorithm the amplitude is estimated as a linear combination of 10 samples, s_i:

$$\hat{\mathcal{A}} = \sum_{i=0}^{9} w_i s_i, \tag{4.1}$$

where the weights w_i are calculated by minimizing the variance of $\hat{\mathcal{A}}$. This algorithm was developed to provide an optimal reduction of the electronics noise and a dynamic subtraction of the pedestal, which is estimated on an event-by-event basis by the average of the presamples.

The LHC Run 2 conditions placed stringent requirements on the ECAL pulse reconstruction algorithm. Several methods were investigated to mitigate the effect of the increased OOT pileup, to achieve optimal noise performance. The methods that were studied included: using a single sample at the signal pulse maximum, a deconvolution method converting the discrete time signal into the

2020 JINST 15 P10002

frequency domain [10], and the multifit. The first one uses a minimal information from the pulse shape and, although being robust against OOT pileup, results in a degradation of energy resolution for most of the energy range below ≈100 GeV. The second was the subject of a pilot study and was never fully developed. The last one is the subject of this paper.

4.2 The multifit algorithm

The multifit method uses a template fit with N_{BX} parameters, comprising one in-time (IT) and up to nine OOT amplitudes, up to five occurring before, and up to four after the IT pulse: $N_{\mathrm{BX}} \in [1\text{–}10]$. The fit minimizes the χ^2 defined as:

$$\chi^2 = \left(\sum_{j=0}^{N_{\mathrm{BX}}} A_j \vec{p}_j - \vec{S}\right)^T \mathbf{C}^{-1} \left(\sum_{j=0}^{N_{\mathrm{BX}}} A_j \vec{p}_j - \vec{S}\right), \tag{4.2}$$

where the vector $\vec{S}$ comprises the 10 readout samples, s_i, after having subtracted the pedestal value, $\vec{p}_j$ are the pulse templates for each BX, and A_j, which are obtained by the fit, are the signal pulse amplitudes in ten consecutive BXs, with A_5 corresponding to the IT BX. The pulse templates $\vec{p}_j$ for each BX have the same shape, but are shifted in time by j multiples of 25 ns. The pulse templates are described by binned distributions with 15 bins of width 25 ns. An extension of five additional time samples after the 10^{th} sample (the last digitized one) is used to obtain an accurate description of the contribution to the signal from early OOT pulses with tails that overlap the IT pulse.

The total covariance matrix $\mathbf{C}$ used in the χ^2 minimization of eq. (4.2) includes the correlation of the noise and the signal between the different time samples. It is defined as the quadratic sum of two contributions:

$$\mathbf{C} = \mathbf{C}_{\mathrm{noise}} \oplus \sum_{j=0}^{N_{\mathrm{BX}}} A_j^2 \mathbf{C}_{\mathrm{pulse}}^j, \tag{4.3}$$

where $\mathbf{C}_{\mathrm{noise}}$ is the covariance matrix associated with the electronics noise and $\mathbf{C}_{\mathrm{pulse}}^j$ is the one associated with the pulse shape template. Each channel of the ECAL, i.e., a crystal with its individual readout, is assigned its own covariance matrix. Quadratic summation of the two components is justified since the variance for the pulse templates is uncorrelated with the electronic noise. In fact, the uncertainty in the shape of the signal pulses for a given channel is dominated by event-by-event fluctuations of the beam spot position along the z-axis, of order several cms [11], which affect the arrival time of particles at the front face of ECAL.

The $\mathbf{C}_{\mathrm{pulse}}$ matrix is calculated as:

$$C_{\mathrm{pulse}}^{i,k} = \frac{\sum_{n=1}^{N_{\mathrm{events}}} \tilde{s}_i(n)\tilde{s}_k(n)}{N_{\mathrm{events}}}, \tag{4.4}$$

where the $\tilde{s}_i(n)$ are the pedestal-subtracted sample values, $s_i(n) - P$, scaled for each event n, such that $\tilde{s}_5(n) = 1$. The value of P equals the average of the three unscaled presamples over many events. Both the templates and their covariance matrices are estimated from collision data and may vary with time, for reasons described in section 5.1. The electronics noise dominates the uncertainty for low-energy pulses, whereas the uncertainty in the template shape dominates for higher energies.

2020 JINST 15 P10002

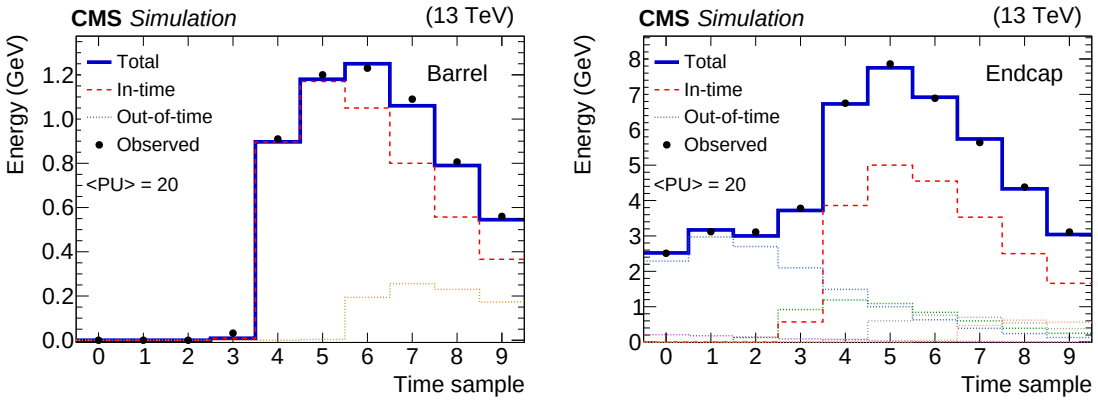

Figure 1. Two examples of fitted pulses for simulated events with 20 average pileup interactions and 25 ns bunch spacing. Signals from individual crystals are shown. They arise from a $p_T = 10$ GeV photon shower in the barrel (left) and in an endcap (right). In the left panel, one OOT pulse, in addition to the IT pulse, is fitted. In the right panel, six OOT pulses, in addition to the IT pulse, are fitted. Filled circles with error bars represent the 10 digitized samples, the red dashed distributions (dotted multicolored distributions) represent the fitted in-time (out-of time) pulses with positive amplitudes. The solid dark blue histograms represent the sum of all the fitted contributions. Within the dotted distributions, the color distinguishes the fitted out-of-time pulses with different BX, while the legend represent them as a generic gray dotted line.

The determination of $\mathbf{C}_{\text{noise}}$, which is calculated analogously as $\mathbf{C}_{\text{pulse}}$, but with dedicated data, is described in section 5.2.

The minimization of the χ^2 in eq. (4.2) has to be robust and fast to use both in the offline CMS reconstruction and at the HLT. In particular, the latter has tight computation time constraints, especially in the EB, where the number of channels that are read out (typically 1000 and as high as 4000) for every triggered BX, poses a severe limitation on the time allowed for each minimization. Therefore, the possibility of using minimization algorithms like MINUIT [12] to perform the 10×10 matrix inversion is excluded. Instead, the technique of nonnegative least squares [13] is used, with the constraint that the fitted amplitudes A_j are all positive. The χ^2 minimization is performed iteratively. First, all the amplitudes are set to zero, and one nonzero amplitude at a time is added. The evaluation of the inverse matrix $\mathbf{C}^{-1}$, which is the computationally intensive operation, is iterated until the χ^2 value in eq. (4.2) converges ($\Delta\chi^2 < 10^{-3}$) [14]. Usually the convergence is reached with fewer than 10 nonzero fitted amplitudes, so the system is, in general, over-constrained. Examples of fitted pulses in single crystals of the EB and EE are shown in figure 1 (right) and (left), respectively. They are obtained from a full detector simulation of photons with transverse momentum $p_T = 10$ GeV.

Since the only unknown quantities are the fitted amplitudes, the minimization corresponds to the solution of a system of linear equations with respect to a maximum of 10 nonnegative A_j values. The implementation uses a C++ template linear algebra library, EIGEN [15], which is versatile and highly optimized. The time required to compute the amplitude of all the channels in one event is approximately 10 ms for typical Run 2 events where the bunch spacing was 25 ns and there is an average of 40 PU interactions per BX. The timing has been measured on an Intel Xeon E5-2650v2 processor, which was used for the benchmark tests of the CMS HLT farm at the beginning of Run 2

2020 JINST 15 P10002

in 2015 [16]. The CPU time needed is about 100 times less than that which was used to perform the equivalent minimization using MINUIT, and for all events is much less than the maximum time of 100 ms/event allowed for the HLT. The algorithm implementation has also been adapted for execution on GPUs for the new processor farm, which will be used for LHC Run 3, which is planned to begin in 2022.

5 Determination of the multifit parameters

5.1 Pulse shape templates

The templates for the $\vec{p}_j$ term in eq. (4.2) are histograms with 15 bins, and represent the expected time distribution of a signal from an energy deposit in the ECAL crystals. The first 10 bins correspond to the samples that are read out in a triggered event. Bins 10–14 describe the tail of the signal pulse shape.

The pulse template differs from crystal to crystal, both because of intrinsic pulse shape differences and, more importantly, because of differences in the relative time position of the pulse maximum, T_{max}, between channels. The pulse templates have also been found to vary with time, during Run 2, as a result of crystal irradiation. Both of these effects must be corrected for, and the time variation requires regular updates to the pulse shape templates during data taking.

The pulse templates are constructed in situ from collision data acquired with a zero-bias trigger, i.e., a beam activity trigger [9], and events recorded with a dedicated high-rate calibration data stream [17]. In the calibration data stream, the ten digitized samples from all single-crystal energy deposits above a predefined noise threshold are recorded, while the rest of the event is dropped to limit the trigger bandwidth. The energy deposits in these events receive contributions from both IT and OOT interactions. In a fraction of the LHC fills, the circulating beams are configured so that a few of the bunch collisions are isolated, i.e., occur between bunches that are not surrounded by other bunches. In these collisions, the nominal single-bunch intensity is achieved without OOT pileup, so a special trigger requirement to record them was developed. This allows a clean measurement of the templates of IT pulses only. An amplitude-weighted average pulse template is obtained, and only hits with amplitudes larger than approximately five times the root-mean-square spread of the noise are used.

During 2017, the pulse templates were recalibrated about 30 times. The LHC implemented collisions with isolated bunches only when the LHC was not completely filled with bunches, during the intensity ramp up, typically at the beginning of the yearly data taking and after each technical stop, i.e., a scheduled period of several days without collisions exploited by the LHC for accelerator developments. For all other updates, normal bunch collisions were used. For these, a minimum amplitude threshold was imposed at the level of 1 GeV, or $5\sigma_{\text{noise}}$ when this was greater, and the amplitude-weighted average of the templates suppressed the relative contribution of OOT PU pulses. It was verified that the pulse templates derived from isolated bunches are consistent with those obtained from nonisolated bunches. Anomalous signals in the APDs, which have a distorted pulse shape, are rejected on the basis of the single-crystal timing and the spatial distribution of the energy deposit among neighboring crystals [17, 18].

The average pulse shape measured in the digitized time window of 10 BXs is extended by five additional time samples to model the falling tail of the pulse, which is used to fit for the

2020 JINST 15 P10002

contribution of early OOT pileup. This is achieved by fitting the average template with a function of the form [19]:

$$A(t) = A\left(1 + \frac{\Delta t}{\alpha\beta}\right)^{\alpha} e^{-\Delta t/\beta} \tag{5.1}$$

where A represents the hit amplitude, $\Delta t = t - T_{\max}$ the time position relative to the peak, and α, β are two shape parameters. Examples of two average pulse shapes, obtained using this method, are shown in figure 2. The extrapolation of the pulse templates outside of the readout window was checked by injecting laser light into the crystals, with a shifted readout phase. The tail of the pulse, measured in this way, agrees with the extrapolated templates.

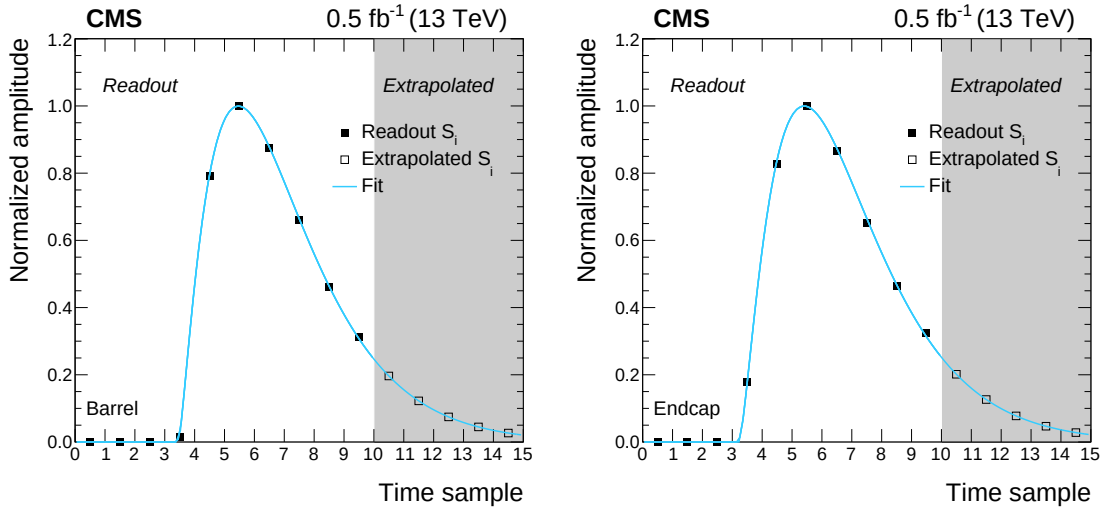

Figure 2. Pulse shape binned templates, measured in collision data recorded during June 2017 in a typical LHC fill, for a channel in the barrel (left) and in an endcap (right). The first 3 bins are the pedestal samples, and their values equal zero by construction. The following 7 bins are estimated from the average of the digitized samples on many hits, while the rightmost 5 bins are estimated by extrapolating the distribution using the function of eq. (5.1) (blue solid line).

The covariance matrix associated with the pulse template, $\mathbf{C}_{\text{pulse}}$, is computed using eq. (4.4), with the same sample of digitized templates used to determine the average pulse template and with the same normalization and weighting strategy. The correlation matrix of the pulse template, $\boldsymbol{\rho}_{\text{pulse}}$, shown in figure 3, is defined as $\rho^{i,k}_{\text{pulse}} = C^{i,k}_{\text{pulse}}/(\sigma^{i}_{\text{pulse}}\sigma^{k}_{\text{pulse}})$, where $\sigma^{i,k}_{\text{pulse}}$ is the square root of the variance of the pulse shape for the i,k bin of the template. The values of $\sigma^{i}_{\text{pulse}}$ are in the range $\left[5\times10^{-4}\text{–}1\times10^{-3}\right]$, the largest values relative to samples in the tail of the pulse template. The elements of the covariance matrix outside the digitization window, $C_{\text{pulse}}{}^{i,k}$ with $i > 9$ or $k > 9$, are estimated from simulations of single-photon events with the interaction time shifted by an integer number of BXs. It was checked that this simulation reproduces well the covariance matrix for the samples inside the readout window.

The $\mathbf{C}_{\text{pulse}}$ matrix shows a strong correlation between the time samples within either the rising edge or the falling tail of the pulse. An anti-correlation is also observed between the time samples of the rising edge and of the falling tail that is mostly due to the spread in the particle arrival time

2020 JINST 15 P10002

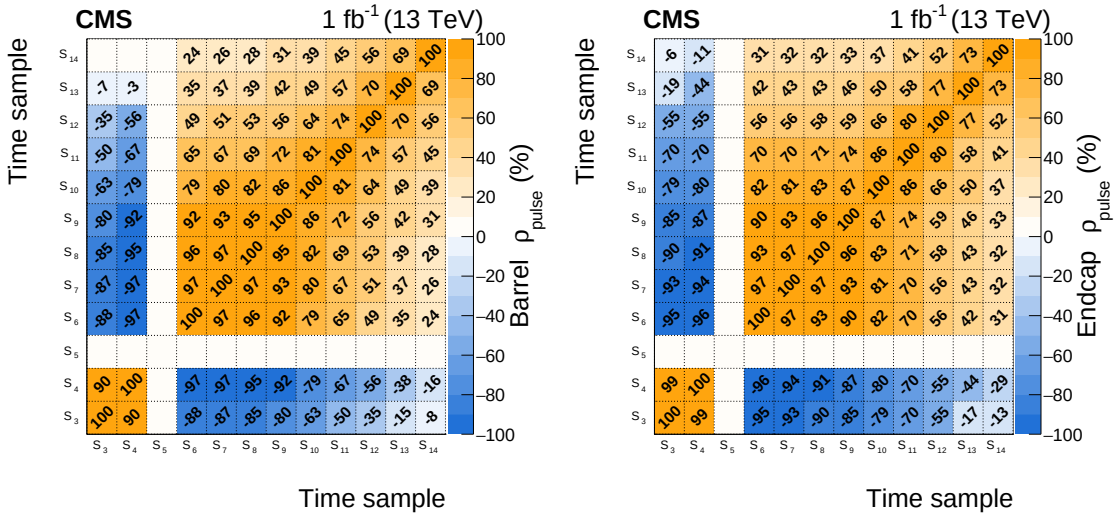

Figure 3. Correlation matrix of the pulse shape binned templates, $\boldsymbol{\rho}_{\text{pulse}}$, measured in collision data recorded during June 2017 in a typical LHC fill, for one channel in the barrel (left) and in an endcap (right). The elements with $i = 5$ or $k = 5$ have zero variance by definition, since $S_5 = 1$ for all the hits. The elements $\rho^{i,k}_{\text{pulse}}$ with $i < 3$ or $k < 3$ are the presamples, where no signal is expected, and are set to zero. Those with $i > 9$ or $k > 9$ are estimated from simulations with a shifted BX. The others are measured in collision data, as described in the text. All the $\rho^{i,k}_{\text{pulse}}$ values in the figure are expressed in percent for legibility.

at the ECAL surface, which reflects the spatial and temporal distribution of the LHC beam spot in CMS [20]. For the measured samples, the correlations between S_9 and S_8, S_7, S_6, are all close to 1, with values in the range (0.90–0.97). For the extrapolated samples, the correlations change from bin to bin: between S_{14} and S_{13}, S_{12}, S_{11} they are 0.69, 0.56, 0.45, respectively, in the case of the barrel.

5.2 Pedestals and electronic noise

The pedestal mean is used in the multifit method to compute the pedestal-subtracted template amplitudes A_j in eq. (4.2). A bias in its measurement would reflect almost linearly in a bias of the fitted amplitude, as discussed in section 6.

The covariance matrix associated with the electronic noise enters the total covariance matrix of eq. (4.3). It is constructed as $\mathbf{C}_{\text{noise}} = \sigma^2_{\text{noise}}\boldsymbol{\rho}_{\text{noise}}$, where σ_{noise} is the measured single-sample noise of the channels, and $\boldsymbol{\rho}_{\text{noise}}$ is the noise correlation matrix. The $\mathbf{C}_{\text{noise}}$ is calculated with eq. (4.4), where i, k are the sample indices, $\tilde{s}_i$ and $\tilde{s}_j$ are the measured sample values, normalized to $\tilde{s}_5$, and P is the expected value in the absence of any signal, calculated, as for eq. (4.4), by averaging the three unscaled presamples over many events. Each element of the noise covariance matrix is the mean over a large number of events. The noise correlation matrix is defined as:

$$\rho^{i,k}_{\text{noise}} = \frac{C^{i,k}_{\text{noise}}}{\sigma^{i}_{\text{noise}}\sigma^{k}_{\text{noise}}}. \tag{5.2}$$

The average pedestal value and the electronic noise are measured separately for the three MGPA gains. For the highest gain value, data from empty LHC bunches [3, 4] are used. These are obtained

2020 JINST 15 P10002

by injecting laser light into the ECAL crystals in coincidence with the bunch crossings. This gain value is used for the vast majority of the reconstructed pulses (up to 150 GeV), and is very sensitive to the electronics noise. One measurement per channel is acquired approximately every 40 minutes. For the other two MGPA gains, the pedestal mean and its fluctuations are measured from dedicated runs without LHC beams present.

The time evolution of the pedestal mean in the EB during Run 2 is shown for the highest MGPA gain in figure 4 (left). A long-term, monotonic drift upwards is visible. Short term (interfill) luminosity related effects are also visible. The short-term variations are smaller when the LHC luminosity is lower. The long-term drift depends on the integrated luminosity, while the short-term effects depend on the instantaneous luminosity, and related to variations inside the readout electronics. The behavior of the variation of the pedestal value with time is similar at any $|\eta|$ of the crystal, while the magnitude of it increases with the pseudorapidity, reflecting the higher irradiation.

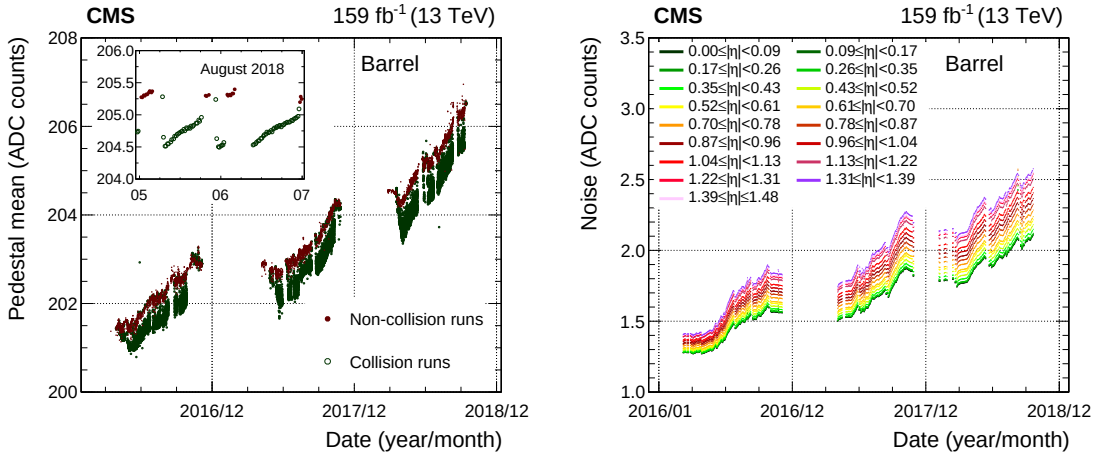

Figure 4. History of the pedestal mean value for the ECAL barrel (left) and its noise (right), measured for the highest MGPA gain in collision or noncollision runs taken during the 2016–2018 data taking period. The inset in the left panel shows an enlargement of two days in August 2018, to show in more detail the variation of the pedestal mean during LHC fills.

The evolution of the electronic noise in the barrel is shown in figure 4 (right). It shows a monotonic increase with time, related to the increase of the APD dark current due to the larger radiation dose; no short-term luminosity-related effects are visible. For the barrel, where 1 ADC count $\cong$ 40 MeV, this translates to an energy-equivalent noise of about 65 MeV at the beginning of 2017 and 80 MeV at the end of the proton-proton running in the same year. A small decrease in the noise induced by the APD dark current is visible after long periods without irradiation, i.e., after the year-end LHC stops. For the endcaps, the single-channel noise related to the VPT signal does not evolve with time, and is approximately 2 ADC counts. Nevertheless, the energy-equivalent noise increases with time and with absolute pseudorapidity $|\eta|$ of the crystal because of the strong dependence of the crystal transparency loss on $|\eta|$ and time, due to higher irradiation level. Consequently, the average noise at the end of 2017 in the endcaps translates to roughly 150 MeV up to $|\eta| \approx 2$, whereas it increases to as much as 500 MeV at the limit of the CMS tracker acceptance ($|\eta| \approx 2.5$). Thus, the relative contribution of $\mathbf{C}_{\text{noise}}$ in the total covariance matrix

2020 JINST 15 P10002

strongly depends on $|\eta|$. For hits with amplitude larger than ≈20 ADC counts, equivalent to an energy ≈1 GeV before applying the light transparency corrections, $\mathbf{C}_{\text{pulse}}$ dominates the covariance matrix for the whole ECAL.

The covariance matrix for the noise used in the multifit is obtained by multiplying the time independent correlation matrix in eq. (5.2) by the time dependent squared single sample noise, σ^2_{noise}. The time evolution is automatically accounted for by updating the values in the conditions database [21], with the measurements obtained in situ.

Correlations between samples exist because of (1) the presence of low-frequency (less than 4 MHz) noise that has been observed during CMS operation [19], and (2) the effect of the feedback resistor in the MGPA circuit [22]. The correlation matrix of the electronic noise was measured with dedicated pedestal runs; it is very similar for all channels within either the EB or the EE, and stable with time. Consequently, it has been averaged over all the channels within a single subsystem. The matrix for the highest gain of the MGPA is shown in figure 5. The MGPA component of the noise is such that the correlation depends almost solely on the time distance between the two samples, following an exponential relationship. For $\Delta t > 100$ ns, it flattens to a plateau corresponding to the low frequency noise.

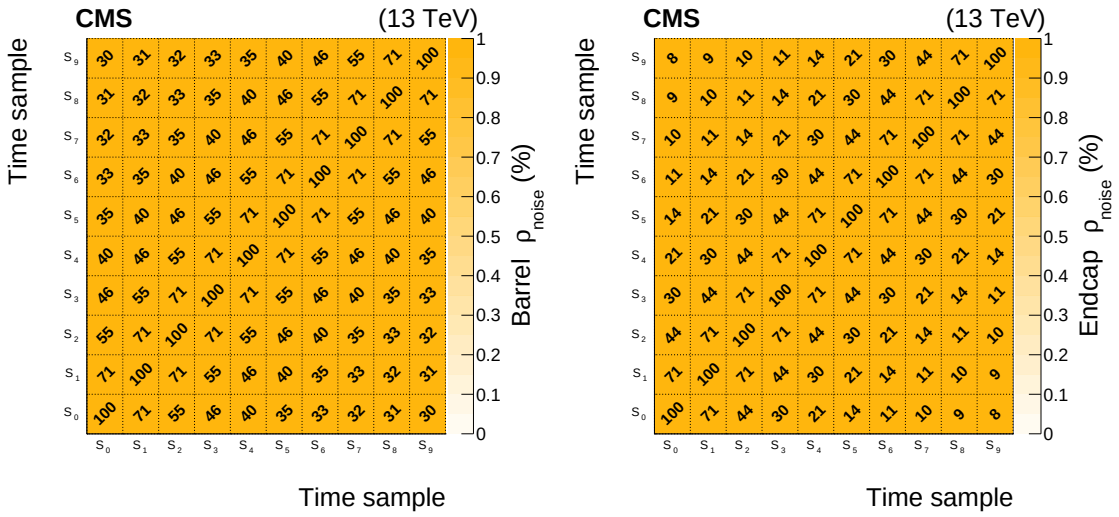

Figure 5. Correlation matrix of the electronics noise, $\boldsymbol{\rho}_{\text{noise}}$, measured in dedicated pedestal runs in Run 2, averaged over all the channels of the barrel (left) or endcaps (right). All the $\rho^{i,k}_{\text{noise}}$ values in the figure are expressed in percent for legibility.

6 Sensitivity of the amplitude reconstruction to pulse timing and pedestal drifts

The multifit amplitude reconstruction utilizes as inputs pedestal baseline values and signal pulse templates that are determined from dedicated periodic measurements. Thus, it is sensitive to their possible changes with time.

Figure 6 shows the absolute amplitude bias for pulses corresponding to a 50 GeV energy deposit (E) in one crystal in the barrel, as a function of the pedestal baseline shift. The dependence for

2020 JINST 15 P10002

deposits in the endcaps is the same. A shift of ±1 ADC count produces an amplitude bias up to 0.3 ADC counts in a single crystal, corresponding, in the barrel, to an energy-equivalent shift of about 300 MeV in a 5×5 crystal matrix. Since the drift of the pedestal baseline with time can be as much as 2 ADC counts in one year of data taking, as shown in figure 4 (left), and is coherent in all crystals, the induced bias is significant, in the range ≈(0.5–1)%, even in the typical energy range of decay products of the W, Z, and Higgs bosons. Therefore, it is important to monitor and periodically correct the pedestals in the reconstruction inputs.

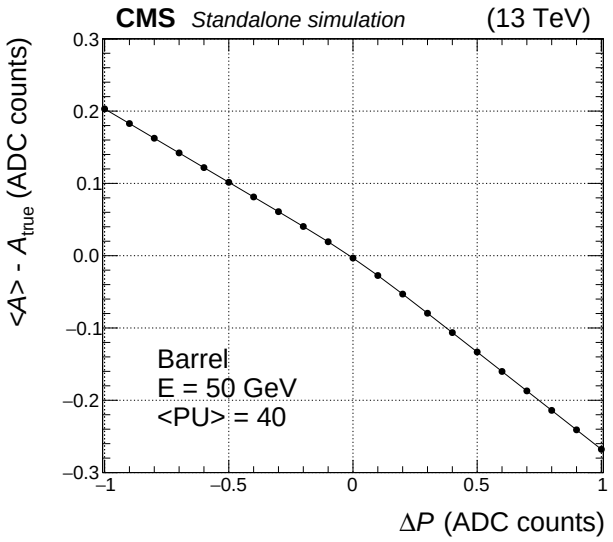

Figure 6. Reconstructed amplitude bias for the IT amplitude, $\langle A \rangle - A_{\text{true}}$, as a function of pedestal shifts ΔP, for a single-crystal pulse of $E = 50$ GeV in the EB.

The IT amplitude resulting from the χ^2 minimization of eq. (4.2) is also more sensitive to a shift in the position of the maximum, T_{max} of the signal pulse, compared to that obtained from the weights method [5]. This timing shift can be caused by variations of the pulse shapes over time, both independently from crystal to crystal and coherently, as discussed in section 5.1. A difference in the pulse maximum position between the measured signal pulse and the binned template will be absorbed into the χ^2 as nonzero OOT amplitudes, A_j, with $j \neq 5$.

To estimate the sensitivity of the reconstructed amplitude to changes in the template timing ΔT_{max}, the amplitude of a given pulse is reconstructed several times, with increasing values of ΔT_{max}. The observed changes in the ratio of the reconstructed amplitude to the true amplitude, $\langle A \rangle / A_{\text{true}}$, as a function of ΔT_{max}, for single-crystal pulses of 50 GeV in the EB and EE, are shown in figure 7 (left) and (right), respectively. The difference in shape for positive and negative time shifts is related to the asymmetry of the pulse shape with respect to the maximum: spurious OOT amplitudes can be fitted more accurately using the time samples preceding the rising edge, where pedestal-only samples are expected, compared to using those on the falling tail. For positive ΔT_{max}, the net change is positive because the effect of an increase in the IT contribution is larger than the decrease in the signal amplitude caused by the misalignment of the template. The change in reconstructed amplitude at a given ΔT_{max} is similar for the barrel and the endcaps. Small differences

2020 JINST 15 P10002

arise mostly from the slightly different rise time of the barrel and endcap pulses and the difference in energy distributions from PU interactions in a single crystal in the two regions. For the endcaps, the residual offset of ≈0.2% for $\Delta T_{\text{max}} = 0$ has two sources. First, the larger occupancy of OOT pileup amplitudes per channel contributes energy coherently to all of the samples within the readout window. Second, the higher electronics noise leads to a looser amplitude constraint in the χ^2 minimization of eq. (4.2), allowing a larger amplitude to be fitted. This offset is reabsorbed in the subsequent absolute energy calibration and it does not affect the energy resolution.

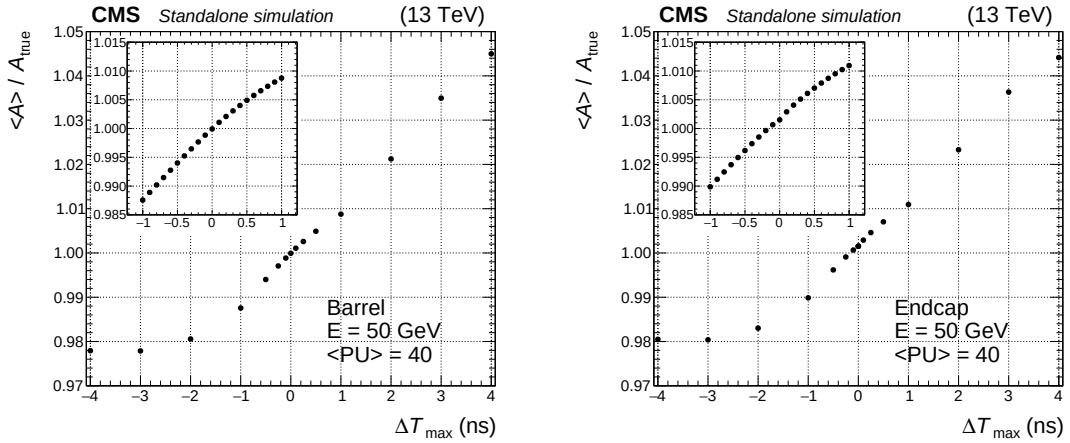

Figure 7. Reconstructed amplitude over true amplitude, $\langle A \rangle / A_{\text{true}}$, as a function of the timing shift of the pulse template, ΔT_{max}, for a single-crystal pulse of $E = 50\,\text{GeV}$ in the EB (left) and EE (right). The insets show an enlargement in the ±1 ns range with a finer ΔT_{max} granularity.

The effects of small channel-dependent differences between actual pulse shapes and the assumed templates are absorbed by the crystal-to-crystal energy intercalibrations. However, any changes with time in the relative position of the template will affect the reconstructed amplitudes, worsening the energy resolution. This implies the need to monitor T_{max} and periodically correct the templates for any observed drifts. The average correlated drift of T_{max} was constantly monitored throughout Run 2, measured with the algorithm of ref. [23]. Its evolution during 2017 is shown in figure 8. The coherent variation can be up to 1 ns. The repeated sharp changes in T_{max} occur when data taking is resumed after a technical stop of the LHC. They are caused by a partial recovery in crystal transparency while the beam is off, followed by a rapid return to the previous value when irradiation resumes. A similar trend was measured in the other years of data-taking during Run 2.

The measured time variation is crystal dependent, since the integrated radiation dose depends on the crystal position, and since there are small differences in the effect between crystals at the same η. For this reason the pulse templates are measured in situ multiple times during periods with collision data, and a specific pulse template is used for each channel. The measurement described in section 5.1 is repeated after every LHC technical stop, when a change of the templates is expected because of partial recovery of the crystal transparency, or when the $|\Delta T_{\text{max}}|$ was larger than 250 ps.

2020 JINST 15 P10002

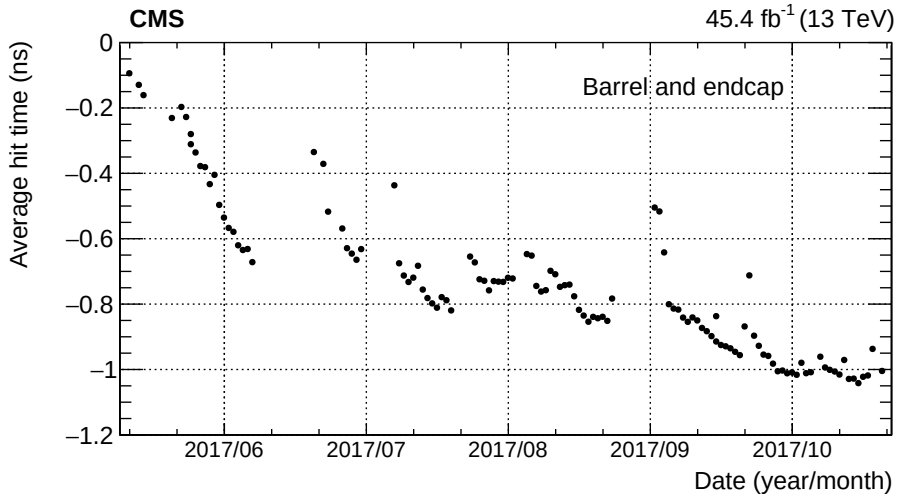

Figure 8. Average timing of ECAL pulses in proton-proton collisions collected in 2017, as measured in ref. [23]. For each point, the average of the hits reconstructed in all barrel and endcaps channels is used. The sharp changes in T_{max} correspond to restarts of data taking following LHC technical stops, as discussed in the text. At the beginning of the yearly data taking, the timing is calibrated so that the average $T_{\text{max}} = 0$.

7 Performance with simulations and collision data

In this section, the performance of the ECAL local reconstruction with the multifit algorithm is compared with the weights method [5]. Simulated events with a PU typical of Run 2 (a Poisson distribution with a mean of 40) and collision data collected in 2016–2018 are used. The data comparisons are performed for low-energy photons from $\pi^0 \to \gamma\gamma$ decays, and for high-energy electrons from $Z \to e^+e^-$ decays.

7.1 Suppression of out-of-time pileup signals

The motivation for implementing the multifit reconstruction is to suppress the OOT pileup energy contribution, while reconstructing IT amplitudes as accurately as possible. To show how well the multifit reconstruction performs, the resolution of the estimated IT energy is compared for single crystals, as a function of the average number of PU interactions. This study was performed using simple pseudo-experiments, where the pulse shape is generated according to the measured template for a barrel crystal at $|\eta| \approx 0$. The appropriate electronics noise, equal to the average value measured in Run 2, together with its covariance matrix, is included. The effect of the PU is simulated assuming that the number of additional interactions has a Poisson distribution about the mean expected value and that these interactions have an energy distribution corresponding to that expected for minimum bias events at the particular value of η of the crystal. The pseudo-experiments are performed for two fixed single-crystal energies: 2 and 50 GeV. For a single crystal, the amplitude is related directly to the energy only through a constant calibration factor, thus the resolution of the uncalibrated amplitude equals the energy resolution. The resolution of a cluster receives other contributions that may degrade the intrinsic single-crystal energy measurement precision, such as a nonuniform

2020 JINST 15 P10002

response across several crystals, within the calibration uncertainties. These considerations are outside the scope of this paper.

The amplitude resolution is estimated as the effective standard deviation σ_{eff}, calculated as half of the smallest symmetrical interval around the peak position containing 68.3% of the events. The PU energy from IT interactions constitutes an irreducible background for both energy reconstruction methods. It is expected that event-by-event fluctuations of this component degrade the energy resolution in both cases as the PU increases. On the other hand, the fluctuations in the energy from all the OOT interactions are suppressed significantly by the multifit algorithm, in contrast to the situation for the weights reconstruction, where they contribute further to the energy resolution deterioration at large average PU. This is shown in figure 9, for the two energies considered in this study. The reconstructed energy is compared with either the true generated energy (corrected for both IT and OOT PU) or the sum of the energy from the IT pileup and the true energy (corrected only for the effect of OOT PU). In the latter case, the amplitude resolution for the multifit reconstruction does not depend on the number of interactions, showing that this algorithm effectively suppresses the contributions of the OOT PU. The offset in resolution in the case of no PU between the two methods, in this ideal case, is due to the improved suppression of the electronic noise resulting from the use of a fixed pedestal rather than the event-by-event estimate used in the weights method. In the data, additional sources of miscalibration may further worsen the energy resolution. Such effects are considered in the full detector simulation used for physics analyses, described below, but are not included in this stand-alone simulation.

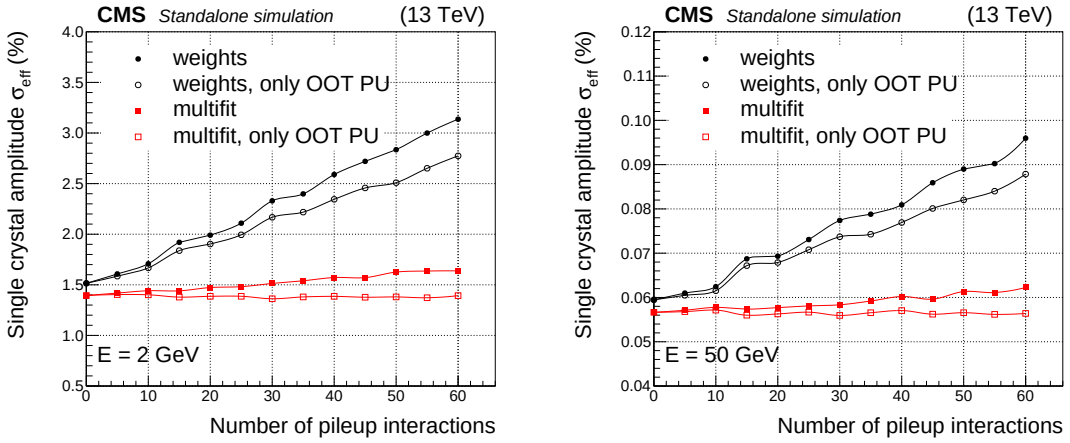

Figure 9. Measured amplitude resolution for two generated energy deposits ($E = 2\,\text{GeV}$ or $E = 50\,\text{GeV}$) in a single ECAL barrel crystal, at $\eta = 0$, reconstructed with either the multifit or the weights algorithm. Filled points show the effective resolution expressed as the difference between the reconstructed energy and the true energy, divided by the true energy. Open points show the percent resolution estimated when the true energy is replaced with the sum of the true energy and the in-time pileup energy.

Simulations performed for an upgraded EB, planned for the high-luminosity phase of the LHC [24], have shown that the multifit algorithm can subtract OOT PU for energies down to the level of the electronic noise, for $\sigma_{\text{noise}} > 10\,\text{MeV}$, for PU values up to 200 with 25 ns bunch spacing. This future reconstruction method will benefit from a more frequent sampling of the pulse

2020 JINST 15 P10002

shape, at 160 MHz, and from a narrower signal pulse to be achieved with the upgraded front-end electronics [25].

7.2 Energy reconstruction with simulated data

The ability of the multifit algorithm to estimate the OOT amplitudes and, consequently, to estimate the IT amplitude is demonstrated in figure 10 (left). Simulated events are generated with an average of 40 PU interactions, with an energy spectrum per EB crystal as shown in figure 10 (right). The reconstructed energy assigned by the multifit algorithm to each BX from −5 to +4 is compared with the generated value. The IT contribution corresponds to BX = 0. Amplitudes are included with energy larger than 50 MeV, a value corresponding approximatively to one standard deviation of the electronic noise [26]. The mode of the distribution of the ratio between the reconstructed and true energies of OOT PU pulses and true energies, $A^{\mathrm{PU}}_{\mathrm{BX}}/A^{\mathrm{true}}_{\mathrm{BX}}$, with BX in the range $[-5,\ldots,+4]$, is equal to unity within ±2.5% for all the BXs. The OOT interactions simulated in these events cover a range from 12 BXs before to 3 BXs after the IT interaction, as is done in the full simulation used in CMS. The distribution of the measured to true energy becomes asymmetric at the boundaries of the pulse readout window (BX = −5, −4, and −3), because the contributions of earlier interactions cannot be resolved with the information provided by the 10 digitized samples. However, this does not introduce a bias in the IT amplitude since the energy contribution from very early BXs below the maximum of the IT pulse is negligible. The remaining offset of ≈0.2% in the median of $A^{\mathrm{PU}}_{\mathrm{BX}}/A^{\mathrm{true}}_{\mathrm{BX}}$ for BXs close to zero is due to the requirement that all the A_j values are nonnegative, i.e., any spuriously fitted OOT pulse can only subtract part of the in-time amplitude. This offset is absorbed in the absolute energy scale calibration and does not affect the energy resolution.

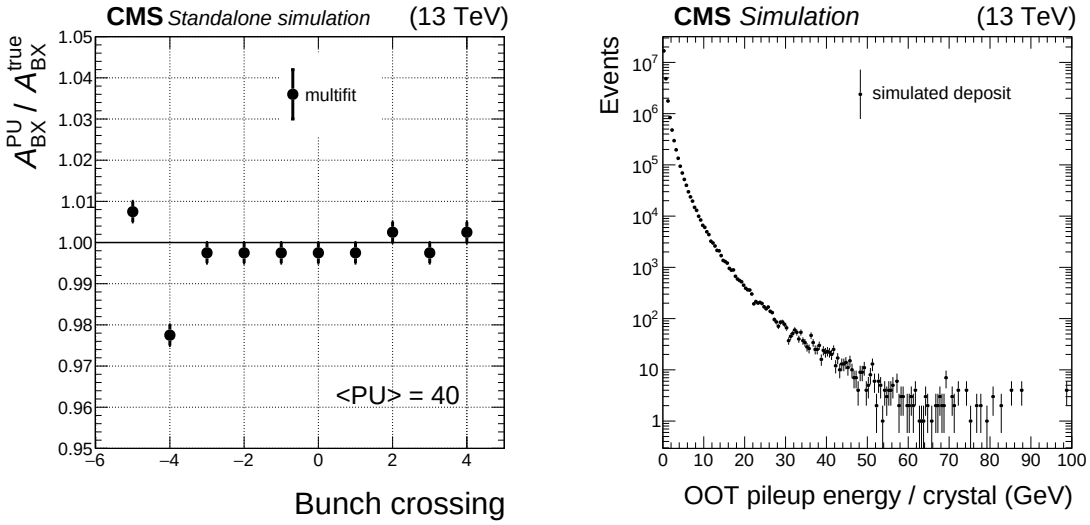

Figure 10. Left: bias in the out-of-time amplitude estimated by the multifit algorithm as a function of BX, for the bunch crossings $-5 \leq \mathrm{BX} \leq +4$. The in-time interaction corresponds to BX = 0 in the figure. The bias is estimated as the mode of the distribution of the ratio between the measured and the true energy. Only statistical uncertainties are shown. Right: energy spectrum in an ECAL barrel crystal, at $\eta \approx 0$.

The energy from an electromagnetic shower for a high-momentum electron or photon is deposited in several adjacent ECAL crystals. A clustering algorithm is required to sum together the

2020 JINST 15 P10002

deposits of adjacent channels that are associated with a single electromagnetic shower. Corrections are applied to rectify the cluster partial containment effects. In the present work, we use a simple clustering algorithm that sums the energy in a 5×5 crystal matrix centered on the crystal with the maximum energy deposit. This approach is adequate for comparing the performance of the two reconstruction algorithms, especially in regions with low tracker material (e.g., $|\eta| < 0.8$), where the fraction of energy lost by electrons by bremsstrahlung (and subsequent photon conversions) is small. Here, more than 95% of the energy is contained in a 5×5 matrix. To reduce the fraction of events with partial cluster containment caused by early bremsstrahlung and photon conversion, a selection is applied to the electrons and photons. In the simulation, events with photon conversions are rejected using Monte Carlo information, whereas in data a variable that uses only information from the tracker is adopted, as described later.

The relative performance of the two reconstruction algorithms is evaluated on a simulated sample of single-photon events generated by GEANT4 with a uniform distribution in η and a flat transverse momentum p_T spectrum extending from 1 to 100 GeV. The photons not undergoing a conversion before the ECAL surface are selected by excluding those that match geometrically electron-positron pair tracks from conversions in the simulation. For the retained photons, the energy is mostly contained in a 5×5 matrix of crystals, and no additional corrections are applied.

The ratio between the reconstructed energy in the 5×5 crystal matrix and the generated photon energy, $E_{5\times5}/E_{\text{true}}$, for nonconverted photons with a uniform distribution in the range $1 < p_T^{\text{true}} < 100$ GeV is histogramed. For both reconstruction algorithms, the distributions show a non-Gaussian tail towards lower values, caused by the energy leakage out of the 5×5 crystal matrix, which is not corrected for. To account for this, σ_{eff}, as defined in section 7.1, is used to quantify the energy resolution. The average energy scale of the reconstructed clusters is shifted downwards for the multifit method, whereas it is approximately unity for the weights reconstruction. As stated earlier, this is because the amplitudes for the OOT pulses (A_j with $j \neq 5$) are constrained to be positive. In the reconstruction of photons used by CMS such a shift is corrected for, a posteriori, by a dedicated multivariate regression, which simultaneously corrects the residual dependence of the energy scale on the cluster containment and IT pileup. This correction is applied in the HLT and, with a more refined algorithm, in the offline event reconstruction. This type of cluster containment correction was developed in Run 1 [26, 27] and has been used subsequently. In this approach, the shift of the $E_{5\times5}/E_{\text{true}}$ distribution is corrected by rescaling the resolution estimator, σ_{eff}, by m, estimated as the mean of a Gaussian function fitting the bulk of the distribution, and expressed in percent. The variation of σ_{eff} as a function of the true p_T of the photon, is shown in figure 11.

The improvement in the precision of the energy measurement is significant for the full range of p_T considered. Expressed as a quadratic contribution to the total, it varies from 10 (15)% in the barrel (endcaps) for photons with $p_T < 5$ GeV, to 0.5 (1.0)% at $p_T = 100$ GeV. The improvement is larger at low p_T, since the relative contribution of the energy deposits from PU interactions, which have the characteristic momentum spectrum shown in figure 10 (right), is relatively larger. This is particularly relevant for suppressing the PU contribution to low-p_T particles that enter the reconstruction of jets and missing transverse momentum with the particle-flow algorithm used in CMS [28], thus preserving the resolution achieved during Run 1 [29–31]. The improvement grows with $|\eta|$ both within the EB and within the EE, because of the increasing probability of overlapping pulses from PU. The improvement is larger in the barrel, even though the PU contribution is smaller

2020 JINST 15 P10002

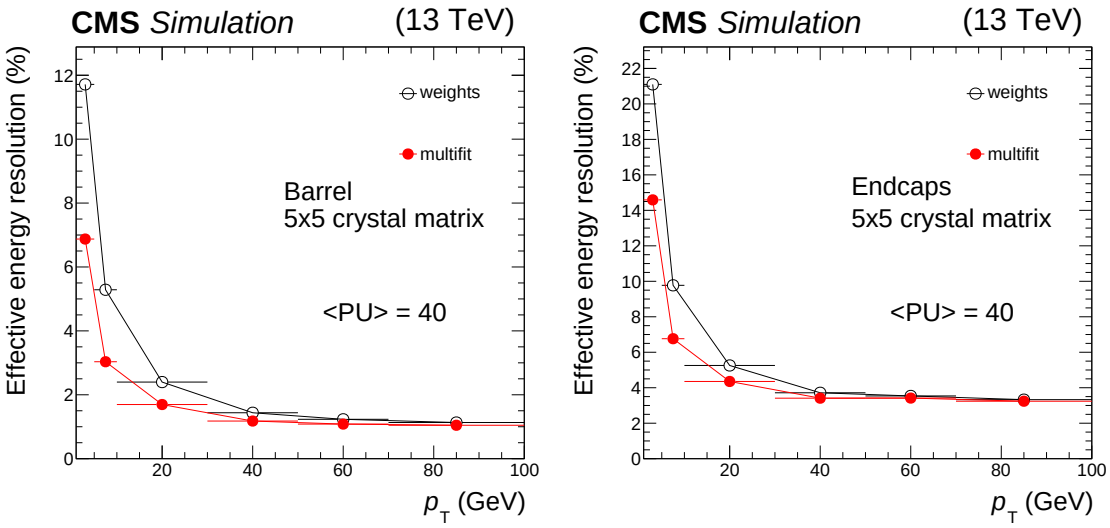

Figure 11. Effective energy resolutions for nonconverted photons in barrel (left) and endcaps (right) as a function of the generated p_T of the photon. The photons are generated with a uniform p_T distribution and their interaction is obtained with the full detector simulation. The average number of PU interactions is 40. The horizontal error bars represent the bin width. The statistical uncertainties are too small to be displayed.

than in the endcaps, because the lower electronic noise allows a more stringent constraint of the amplitudes in the multifit. For photons, the improvement extends above $p_T \approx 50$ GeV, because of the higher number of digitized samples of the pulse shape used, and the suppression of the residual OOT PU contribution. The energy resolution becomes constant at very high energies, above a few hundred GeV, where it is dominated by sources other than the relatively tiny contribution of OOT pileup energy, such as nonuniformities in the energy response of different crystals belonging to the same cluster. The improvement in energy resolution is also expected to be valid for electrons with $p_T > 20$ (10) GeV in the barrel (endcaps), since the electron momentum resolution is dominated by the ECAL cluster measurement above these p_T values [27].

7.3 Energy reconstruction with Run 2 data

7.3.1 Effect on low energy deposits using $\pi^0 \to \gamma\gamma$

The improvement in the energy resolution for low-energy clusters is quantified in data using π^0 mesons decaying into two photons. The p_T spectrum of the photons, selected by a dedicated calibration trigger [17], falls very fast and most of the photons have a p_T in the range of 1–2 GeV. The photon energy in this case is reconstructed summing the energy of the crystals in a 3×3 matrix. Figure 12 shows the diphoton invariant masses when both clusters are in the EB (left) and when both are in EE (right). The invariant mass distributions obtained with the weights and the multifit methods are compared, using a subset of the π^0 calibration data collected during 2018. The position of the peak, M, is affected by OOT PU differently in the multifit method and in the weights algorithm. Since the $\pi^0 \to \gamma\gamma$ process is only used to calibrate the relative response of a crystal with respect to others, the absolute energy scale is not important here. The energy scale is determined separately by comparing the position of the $Z \to e^+e^-$ mass peak in data and

2020 JINST 15 P10002

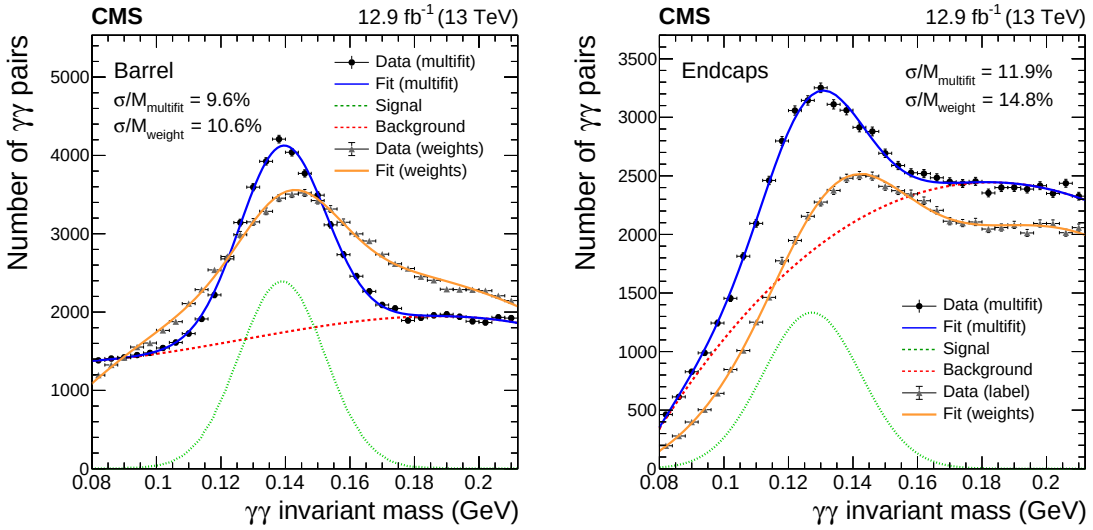

Figure 12. The invariant mass distribution of the two photons for the selected $\pi^0 \to \gamma\gamma$ candidates in the barrel (left) and endcaps (right), for the single-crystal amplitudes measured with either the weights or the multifit reconstruction. A portion of collision data with typical Run 2 conditions, recorded during July 2018, is used. Vertical error bars represent the statistical uncertainty. The result of the fit with a Gaussian distribution (green dotted line) plus a polynomial function (red dashed line) is superimposed on the measured distributions for the multifit case (dark blue solid line). For the weights case the same model is used, but only the total likelihood is shown superimposed (light orange solid line).

simulation. On the other hand, the improvement in mass resolution, σ/M, is significant, 4.5% (8.8%) in quadrature in the barrel (endcaps).

At the end of 2017, the LHC operated for a period of about 1 month with a filling scheme with trains of 8 bunches alternated with 4 empty BXs. The resilience of the multifit method to OOT pileup had a particularly positive effect in this period, since the bunch-to-bunch variations in OOT PU are larger than with the standard LHC filling schemes used in Run 2. All the bunches of a given train provide approximately the same luminosity, about $5.5{\times}10^{27}\,\mathrm{cm}^{-2}\,\mathrm{s}^{-1}$, so the average number of PU interactions is the typical one of Run 2 (about 34, with peaks up to 80). Data from this period is used to assess the sensitivity of the algorithms to OOT interactions by estimating the invariant mass peak position of the π^0 mesons as a function of BX within each LHC bunch train. The measured invariant mass, normalized to that measured in the first BX of the train, is shown in figure 13 (left). The peak position, estimated with the weights algorithm, increases for BXs towards the middle of the bunch train, where the contribution from OOT collisions is larger, and then decreases again towards the end of the train. In contrast, for the multifit reconstruction, the peak position remains stable within ±0.4% with respect to the value observed in the first BX of the train. The overall resolution in the diphoton invariant mass improves significantly using the multifit algorithm, and, within the precision of the measurement, is insensitive to the variations of OOT PU for different BX within the train. This is shown in figure 13 (right).

7.3.2 Effect on high energy deposits using $Z \to e^+e^-$

The performance of the two algorithms for high-energy electromagnetic deposits is estimated using electrons from $Z \to e^+e^-$ decays. Electrons with $p_T > 25\,\mathrm{GeV}$ are identified with tight electron

2020 JINST 15 P10002

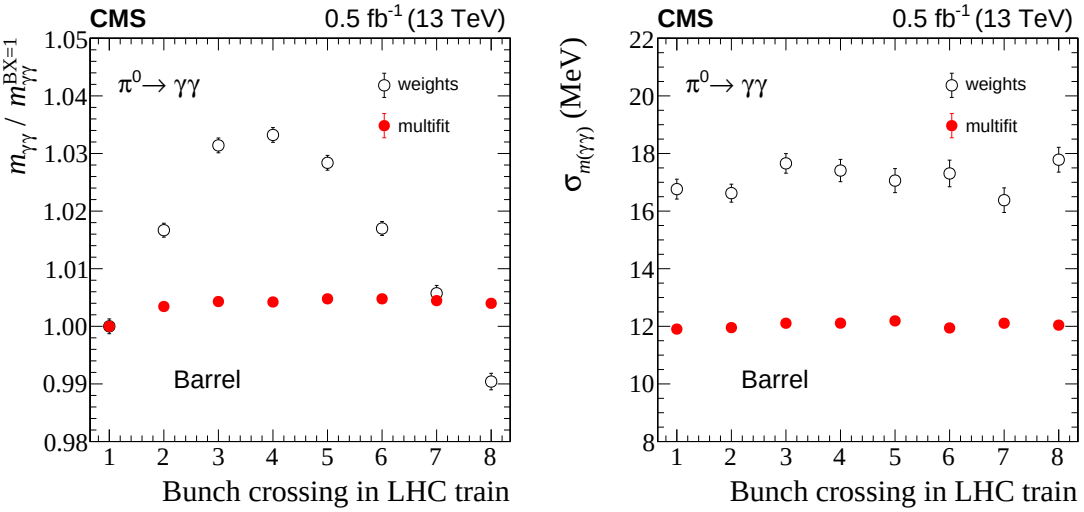

Figure 13. Peak position, normalized to the mass measured in the first BX of the train, (left) and Gaussian resolution $\sigma_{m(\gamma\gamma)}$ (right) of the invariant mass distribution of $\pi^0 \to \gamma\gamma$ decays with both photons in the EB, within a bunch train of 8 colliding bunches from an LHC fill in October 2017. Error bars represent the statistical uncertainty. The single-crystal energy is reconstructed either with the weights method (open circles) or with the multifit method (filled circles). Each point is obtained by fitting the diphoton invariant mass distribution in collisions selected from a single BX of the train.

identification criteria, using a discriminant based on a multivariate approach [27]. To decouple the effects of cluster containment corrections from the single-crystal resolution, 5×5 crystal matrices are used to form clusters. The sample is enriched in low-bremsstrahlung electrons by selecting with an observable using only tracker information, f_{brem}, which represents the fraction of momentum, estimated from the track, lost before reaching the ECAL. It is defined as $f_{\text{brem}} = (p_{\text{in}} - p_{\text{out}})/p_{\text{in}}$, where p_{in} and p_{out} are the momenta of the track extrapolated to the point of closest approach to the beam spot and estimated from the track at the last sensitive layer of the tracker, respectively. The variable f_{brem} is required to be smaller than 20%. In the range $0.8 < |\eta| < 2.5$ [27], the resolution is dominated by the incomplete containment of the 5×5 crystal matrix caused by the larger amount of tracker material in this region. Therefore, detailed performance comparisons are restricted to events with electromagnetic showers occurring in the central region of the EB.

Figure 14 shows the invariant mass of 5×5 cluster pairs, for a portion of the 2016 data, selecting pairs of electrons, e_1 and e_2, that lie within a representative central region of the barrel ($0.200 < \max(|\eta_1|, |\eta_2|) < 0.435$). The outcome is similar in other regions with low tracker material. The shift in the absolute energy scale for the simplified 5×5 clustering, caused by the multifit A_j being nonnegative for each BX, is not corrected for. The improvement is still significant for the p_{T} range characteristic of $Z \to e^+e^-$ decays, matching the expectation from the simulation, shown in figure 11, namely an improvement in resolution of ≈1% in quadrature, after unfolding the natural width of the Z boson, for electrons and photons with $30 < p_{\text{T}} < 100$ GeV.

A full comparison of the performance of the multifit algorithm in Run 2 with that of the weights algorithm in Run 1 would require a reanalysis of the Run 1 data, applying the more sophisticated clustering techniques used in Run 2. Nevertheless, it is instructive to make a straightforward

2020 JINST 15 P10002

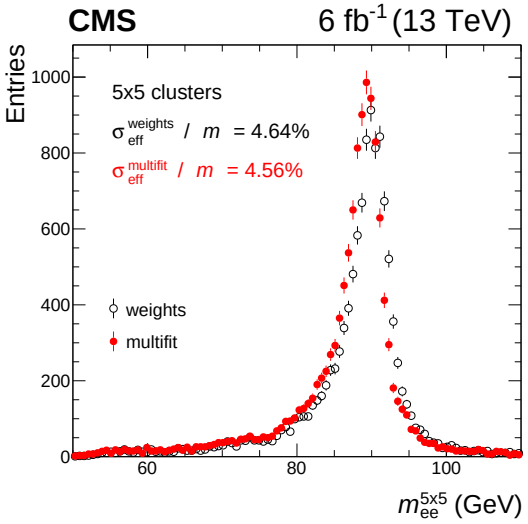

Figure 14. Example of the $Z \rightarrow e^+e^-$ invariant mass distribution in a central region of the barrel ($0.200 < \max(|\eta_1|, |\eta_2|) < 0.435$) with the single-crystal amplitude estimated using either the weights or the multifit method. A portion of collision data with typical Run 2 conditions, recorded during October 2016, is used. Error bars represent the statistical uncertainty. The energy is summed over a 5×5 crystal matrix. The reported values of σ_{eff} include the natural width of the Z boson, and are expressed as a percent of the position of the peak, m, of the corresponding invariant mass distribution.

comparison. For Run 1, where the crystal energy was reconstructed with the default weights method, the electron energy was estimated with the simple 5×5 crystal cluster, and using the optimal calibrations of the 2012 data set ($\sqrt{s}$ = 8 TeV and 50 ns LHC bunch spacing) [27]. The effective resolution of the dielectron invariant mass distribution, normalized to its peak, is $\sigma_{\text{eff}}/m = 4.59\%$. This is consistent with the value of 4.56% obtained in Run 2 with the multifit algorithm, shown in figure 14. This indicates that the multifit method can maintain the ECAL performance obtained during Run 1, in the p_{T} range ≈(5–100) GeV, relevant for most data analyses performed with CMS, despite the substantially larger PU present in Run 2.

7.3.3 Effect on jets

The contribution to the average offset of the jet energy scale, from the reconstructed electromagnetic component of each additional PU interaction, was estimated in a simulated sample of pure noise in the CMS detector by considering the energy contained in cones randomly chosen within the detector acceptance. This shows that the contribution to the offset from ECAL signals is reduced to a value of less than 10%, similar to that obtained in Run 1. Further details are given in ref. [30].

7.4 Reconstruction of cluster shape variables

The relative contribution of the PU energy within a cluster for electrons from Z boson decays is less than for clusters from π^0 meson decays, and the sample of events is smaller. For these reasons, it is difficult to estimate the variation of the energy scale within one LHC fill arising from this contribution. The effect on the cluster shapes is still significant, since they are computed using

2020 JINST 15 P10002

all the hits in a cluster, including the low-energy ones. One example is provided by the evolution, within an LHC fill, of the variable R_9, defined as the ratio of the energy in a 3×3 crystal matrix centered on the seed hit of the cluster, divided by the total energy of the cluster. This variable is an important measure of cluster shape, since it is often used to distinguish between showering or converted photons, and those not undergoing a bremsstrahlung process or conversion within the tracker. For example, in studies of Higgs boson physics, it is used to separate $H \to \gamma\gamma$ events into categories with different $m_{\gamma\gamma}$ effective mass resolutions. Thus it is important that the R_9 variable remains stable over time. Figure 15 shows the median of the R_9 distribution for clusters from electron pairs in the barrel having a mass consistent with that of the Z boson, during an LHC fill in 2016 with an average PU decreasing from a value of 42 at the beginning of the fill to a value of 13 at the end. The stability of the cluster shape as a function of instantaneous luminosity, obtained with the multifit algorithm, is clearly better than the one obtained with the weights reconstruction. The main reason the median R_9 values drift up during a fill is that the denominator of the R_9 ratio, which includes contributions from low-energy hits located outside of the 3×3 matrix, decreases in the weights algorithm when the instantaneous luminosity (and the PU) decreases.

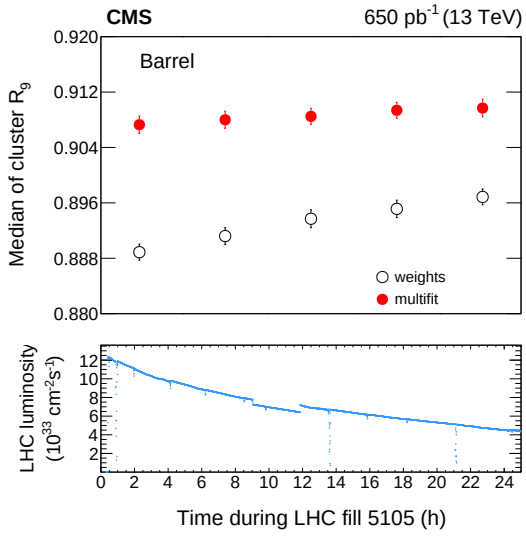

Figure 15. History of the median of the R_9 cluster shape for electrons from $Z \to e^+e^-$ decays during one typical LHC fill in 2016. Hits are reconstructed with either the multifit (filled circles) or the weights algorithm (open circles). Each point represents the median of the distribution for a 5 hour period during the considered LHC fill. Error bars represent the statistical uncertainty on the median. The bottom panel shows the instantaneous luminosity delivered by the LHC as a function of time. The steps in the luminosity occurring about every two hours correspond to changes in the LHC beam crossing angle, which changes the overlap area of the bunches. Larger brief drops could indicate emittance scans during the fill.

Another effect that has been checked in data is the rejection power for anomalous signals ascribed to direct energy deposition in the APDs [18] by traversing particles. Unlike the hits in an electromagnetic shower, the anomalous signals generally occur in single channels of the calorimeter. They are rejected by a combination of a topological selection and a requirement on the hit timing. The topological selection rejects hits for which the value of the quantity $(1 - E_4/E_1)$ is close to 1, where E_1 is the energy of the crystal and E_4 is the energy sum of the four nearest neighboring

2020 JINST 15 P10002

crystals. A simulation of anomalous signals in the APDs is used, and the efficiency is defined as the fraction of the reconstructed hits in crystals with anomalous signals identified as such by the offline reconstruction. The rejection efficiency obtained when using the multifit reconstruction is improved by as much as 15% compared to the weights method for hits with $E < 15\,\text{GeV}$. The probability of rejecting hits from genuine energy deposits has been checked on data with hits within clusters of $\text{Z} \to \text{e}^+\text{e}^-$ and is lower than 10^{-3} over the entire p_T spectrum of electrons from Z boson decays for both methods.

8 Summary

A multifit algorithm that uses a template fitting technique to reconstruct the energy of single hits in the CMS electromagnetic calorimeter has been presented. This algorithm was implemented before the start of the Run 2 data taking period of the LHC, replacing the weights method used in Run 1. The change was motivated by the reduction of the LHC bunch spacing from 50 to 25 ns, and by the higher instantaneous luminosity of Run 2, which led to a substantial increase in both the in-time and out-of-time pileup. Procedures have been developed to provide regular updates of input parameters to ensure the stability of energy reconstruction over time.

Studies based on $\pi^0 \to \gamma\gamma$ and $\text{Z} \to \text{e}^+\text{e}^-$ control samples in data show that the energy resolution for deposits ranging from a few to several tens of GeV is improved. The gain is more significant for lower energy electromagnetic deposits, for which the relative contribution of pileup is larger. This enhances the reconstruction of jets and missing transverse energy with the particle-flow algorithm used in CMS. These results have been reproduced with simulation studies, which show that an improvement relative to the weights method is obtained at all energies, including those relevant for photons from Higgs boson decays.

Simulation studies show that the new algorithm will perform successfully at the high-luminosity LHC, where a peak pileup of about 200 interactions per bunch crossing, with 25 ns bunch spacing, is expected.

Acknowledgments

We congratulate our colleagues in the CERN accelerator departments for the excellent performance of the LHC and thank the technical and administrative staffs at CERN and at other CMS institutes for their contributions to the success of the CMS effort. In addition, we gratefully acknowledge the computing centers and personnel of the Worldwide LHC Computing Grid for delivering so effectively the computing infrastructure essential to our analyses. Finally, we acknowledge the enduring support for the construction and operation of the LHC and the CMS detector provided by the following funding agencies: BMBWF and FWF (Austria); FNRS and FWO (Belgium); CNPq, CAPES, FAPERJ, FAPERGS, and FAPESP (Brazil); MES (Bulgaria); CERN; CAS, MoST, and NSFC (China); COLCIENCIAS (Colombia); MSES and CSF (Croatia); RIF (Cyprus); SENESCYT (Ecuador); MoER, ERC IUT, PUT and ERDF (Estonia); Academy of Finland, MEC, and HIP (Finland); CEA and CNRS/IN2P3 (France); BMBF, DFG, and HGF (Germany); GSRT (Greece); NKFIA (Hungary); DAE and DST (India); IPM (Iran); SFI (Ireland); INFN (Italy); MSIP and NRF (Republic of Korea); MES (Latvia); LAS (Lithuania); MOE and UM (Malaysia); BUAP,

2020 JINST 15 P10002

CINVESTAV, CONACYT, LNS, SEP, and UASLP-FAI (Mexico); MOS (Montenegro); MBIE (New Zealand); PAEC (Pakistan); MSHE and NSC (Poland); FCT (Portugal); JINR (Dubna); MON, RosAtom, RAS, RFBR, and NRC KI (Russia); MESTD (Serbia); SEIDI, CPAN, PCTI, and FEDER (Spain); MOSTR (Sri Lanka); Swiss Funding Agencies (Switzerland); MST (Taipei); ThEPCenter, IPST, STAR, and NSTDA (Thailand); TUBITAK and TAEK (Turkey); NASU (Ukraine); STFC (United Kingdom); DOE and NSF (U.S.A.).

Individuals have received support from the Marie-Curie program and the European Research Council and Horizon 2020 Grant, contract Nos. 675440, 752730, and 765710 (European Union); the Leventis Foundation; the A.P. Sloan Foundation; the Alexander von Humboldt Foundation; the Belgian Federal Science Policy Office; the Fonds pour la Formation à la Recherche dans l'Industrie et dans l'Agriculture (FRIA-Belgium); the Agentschap voor Innovatie door Wetenschap en Technologie (IWT-Belgium); the F.R.S.-FNRS and FWO (Belgium) under the "Excellence of Science — EOS" — be.h project n. 30820817; the Beijing Municipal Science & Technology Commission, No. Z191100007219010; the Ministry of Education, Youth and Sports (MEYS) of the Czech Republic; the Deutsche Forschungsgemeinschaft (DFG) under Germany's Excellence Strategy — EXC 2121 "Quantum Universe" — 390833306; the Lendület ("Momentum") Program and the János Bolyai Research Scholarship of the Hungarian Academy of Sciences, the New National Excellence Program ÚNKP, the NKFIA research grants 123842, 123959, 124845, 124850, 125105, 128713, 128786, and 129058 (Hungary); the Council of Science and Industrial Research, India; the HOMING PLUS program of the Foundation for Polish Science, cofinanced from European Union, Regional Development Fund, the Mobility Plus program of the Ministry of Science and Higher Education, the National Science Center (Poland), contracts Harmonia 2014/14/M/ST2/00428, Opus 2014/13/B/ST2/02543, 2014/15/B/ST2/03998, and 2015/19/B/ST2/02861, Sonata-bis 2012/07/E/ST2/01406; the National Priorities Research Program by Qatar National Research Fund; the Ministry of Science and Higher Education, project no. 02.a03.21.0005 (Russia); the Tomsk Polytechnic University Competitiveness Enhancement Program and "Nauka" Project FSWW-2020-0008 (Russia); the Programa Estatal de Fomento de la Investigación Científica y Técnica de Excelencia María de Maeztu, grant MDM-2015-0509 and the Programa Severo Ochoa del Principado de Asturias; the Thalis and Aristeia programs cofinanced by EU-ESF and the Greek NSRF; the Rachadapisek Sompot Fund for Postdoctoral Fellowship, Chulalongkorn University and the Chulalongkorn Academic into Its 2nd Century Project Advancement Project (Thailand); the Kavli Foundation; the Nvidia Corporation; the SuperMicro Corporation; the Welch Foundation, contract C-1845; and the Weston Havens Foundation (U.S.A.).

References

[1] CMS collaboration, *The CMS Experiment at the CERN LHC*, 2008 *JINST* **3** S08004.

[2] CMS collaboration, *The CMS electromagnetic calorimeter project: Technical Design Report*, CERN-LHCC-97-033 (1997).

[3] M. Anfreville et al., *Laser monitoring system for the CMS lead tungstate crystal calorimeter*, *Nucl. Instrum. Meth. A* **594** (2008) 292.

[4] L.-Y. Zhang, D. Bailleux, A. Bornheim, K.-J. Zhu and R.-Y. Zhu, *Performance of the monitoring light source for the CMS lead tungstate crystal calorimeter*, *IEEE Trans. Nucl. Sci.* **52** (2005) 1123.

2020 JINST 15 P10002

[5] P. Adzic et al., *Reconstruction of the signal amplitude of the CMS electromagnetic calorimeter*, *Eur. Phys. J. C* **46** (2006) 23.

[6] GEANT4 collaboration, *GEANT4 — a simulation toolkit*, *Nucl. Instrum. Meth. A* **506** (2003) 250.

[7] T. Sjöstrand et al., *An introduction to PYTHIA 8.2*, *Comput. Phys. Commun.* **191** (2015) 159 [arXiv:1410.3012].

[8] CMS collaboration, *Event generator tunes obtained from underlying event and multiparton scattering measurements*, *Eur. Phys. J. C* **76** (2016) 155 [arXiv:1512.00815].

[9] CMS collaboration, *The CMS trigger system*, 2017 *JINST* **12** P01020 [arXiv:1609.02366].

[10] S. Gadomski, G. Hall, T. Hogh, P. Jalocha, E. Nygard and P. Weilhammer, *The Deconvolution method of fast pulse shaping at hadron colliders*, *Nucl. Instrum. Meth. A* **320** (1992) 217.

[11] CMS collaboration, *CMS Tracking Performance Results from Early LHC Operation*, *Eur. Phys. J. C* **70** (2010) 1165 [arXiv:1007.1988].

[12] F. James and M. Roos, *Minuit: A System for Function Minimization and Analysis of the Parameter Errors and Correlations*, *Comput. Phys. Commun.* **10** (1975) 343.

[13] D. Chen and R.J. Plemmons, *Nonnegativity constraints in numerical analysis*, in *The Birth of Numerical Analysis*, World Scientific Europe (2009), p. 109.

[14] C.L. Lawson and R.J. Hanson, *Solving least squares problems*, in *Classics in Applied Mathematics*, Society for Industrial and Applied Mathematics (1995).

[15] G. Guennebaud and B. Jacob, *Eigen v3*, (2010) http://eigen.tuxfamily.org.

[16] C. Richardson, *CMS High Level Trigger Timing Measurements*, *J. Phys. Conf. Ser.* **664** (2015) 082045.

[17] CMS collaboration, *Energy Calibration and Resolution of the CMS Electromagnetic Calorimeter in pp Collisions at* $\sqrt{s} = 7$ *TeV*, 2013 *JINST* **8** P9009 [arXiv:1306.2016].

[18] CMS collaboration, *Anomalous APD signals in the CMS Electromagnetic Calorimeter*, *Nucl. Instrum. Meth. A* **695** (2012) 293.

[19] CMS collaboration, *Performance and Operation of the CMS Electromagnetic Calorimeter*, 2010 *JINST* **5** T03010 [arXiv:0910.3423].

[20] CMS collaboration, *CMS luminosity based on pixel cluster counting — Summer 2013 update*, CMS-PAS-LUM-13-00 (2013).

[21] S.D. Guida, G. Govi, M. Ojeda, A. Pfeiffer and R. Sipos, *The CMS Condition Database System*, in proceedings of the *21st International Conference on Computing in High Energy and Nuclear Physics (CHEP 2015)*, Okinawa, Japan, 13–17 April 2015, *J. Phys. Conf. Ser.* **664** (2015) 042024.

[22] Z. Antunovic et al., *Radiation hard avalanche photodiodes for the CMS detector*, *Nucl. Instrum. Meth. A* **537** (2005) 379.

[23] CMS collaboration, *Time Reconstruction and Performance of the CMS Electromagnetic Calorimeter*, 2010 *JINST* **5** T03011 [arXiv:0911.4044].

[24] G. Apollinari et al., *High-Luminosity Large Hadron Collider (HL-LHC)*, in *CERN Yellow Reports: Monographs* **4**, CERN, Geneva Switzerland (2017) [CERN-2017-007-M].

[25] CMS collaboration, *The Phase-2 Upgrade of the CMS Barrel Calorimeters*, CERN-LHCC-2017-011 (2017) [CMS-TDR-015].

[26] CMS collaboration, *Performance of Photon Reconstruction and Identification with the CMS Detector in Proton-Proton Collisions at* $\sqrt{s} = 8$ *TeV*, 2015 *JINST* **10** P08010 [arXiv:1502.02702].

2020 JINST 15 P10002

[27] CMS collaboration, *Performance of Electron Reconstruction and Selection with the CMS Detector in Proton-Proton Collisions at* $\sqrt{s} = 8$ *TeV*, 2015 *JINST* **10** P06005 [arXiv:1502.02701].

[28] CMS collaboration, *Particle-flow reconstruction and global event description with the CMS detector*, 2017 *JINST* **12** P10003 [arXiv:1706.04965].

[29] CMS collaboration, *Jet energy scale and resolution in the CMS experiment in pp collisions at* 8 *TeV*, 2017 *JINST* **12** P02014 [arXiv:1607.03663].

[30] CMS collaboration, *Jet energy scale and resolution performance with* 13 *TeV data collected by CMS in 2016*, CMS-DP-2018-028 (2018).

[31] CMS collaboration, *Performance of missing transverse momentum reconstruction in proton-proton collisions at* $\sqrt{s} = 13$ *TeV using the CMS detector*, 2019 *JINST* **14** P07004 [arXiv:1903.06078].

2020 JINST 15 P10002

The CMS collaboration

Yerevan Physics Institute, Yerevan, Armenia

A.M. Sirunyan[†], A. Tumasyan

Institut für Hochenergiephysik, Wien, Austria

W. Adam, F. Ambrogi, T. Bergauer, M. Dragicevic, J. Erö, A. Escalante Del Valle, R. Frühwirth[1], M. Jeitler[1], N. Krammer, L. Lechner, D. Liko, T. Madlener, I. Mikulec, F.M. Pitters, N. Rad, J. Schieck[1], R. Schöfbeck, M. Spanring, S. Templ, W. Waltenberger, C.-E. Wulz[1], M. Zarucki

Institute for Nuclear Problems, Minsk, Belarus

V. Chekhovsky, A. Litomin, V. Makarenko, J. Suarez Gonzalez

Universiteit Antwerpen, Antwerpen, Belgium

M.R. Darwish[2], E.A. De Wolf, D. Di Croce, X. Janssen, T. Kello[3], A. Lelek, M. Pieters, H. Rejeb Sfar, H. Van Haevermaet, P. Van Mechelen, S. Van Putte, N. Van Remortel

Vrije Universiteit Brussel, Brussel, Belgium

F. Blekman, E.S. Bols, S.S. Chhibra, J. D'Hondt, J. De Clercq, D. Lontkovskyi, S. Lowette, I. Marchesini, S. Moortgat, A. Morton, Q. Python, S. Tavernier, W. Van Doninck, P. Van Mulders

Université Libre de Bruxelles, Bruxelles, Belgium

D. Beghin, B. Bilin, B. Clerbaux, G. De Lentdecker, H. Delannoy, B. Dorney, L. Favart, A. Grebenyuk, A.K. Kalsi, I. Makarenko, L. Moureaux, L. Pétré, A. Popov, N. Postiau, E. Starling, L. Thomas, C. Vander Velde, P. Vanlaer, D. Vannerom, L. Wezenbeek

Ghent University, Ghent, Belgium

T. Cornelis, D. Dobur, M. Gruchala, I. Khvastunov[4], M. Niedziela, C. Roskas, K. Skovpen, M. Tytgat, W. Verbeke, B. Vermassen, M. Vit

Université Catholique de Louvain, Louvain-la-Neuve, Belgium

G. Bruno, F. Bury, C. Caputo, P. David, C. Delaere, M. Delcourt, I.S. Donertas, A. Giammanco, V. Lemaitre, K. Mondal, J. Prisciandaro, A. Taliercio, M. Teklishyn, P. Vischia, S. Wuyckens, J. Zobec

Centro Brasileiro de Pesquisas Fisicas, Rio de Janeiro, Brazil

G.A. Alves, G. Correia Silva, C. Hensel, A. Moraes

Universidade do Estado do Rio de Janeiro, Rio de Janeiro, Brazil

W.L. Aldá Júnior, E. Belchior Batista Das Chagas, H. BRANDAO MALBOUISSON, W. Carvalho, J. Chinellato[5], E. Coelho, E.M. Da Costa, G.G. Da Silveira[6], D. De Jesus Damiao, S. Fonseca De Souza, J. Martins[7], D. Matos Figueiredo, M. Medina Jaime[8], M. Melo De Almeida, C. Mora Herrera, L. Mundim, H. Nogima, P. Rebello Teles, L.J. Sanchez Rosas, A. Santoro, S.M. Silva Do Amaral, A. Sznajder, M. Thiel, E.J. Tonelli Manganote[5], F. Torres Da Silva De Araujo, A. Vilela Pereira

Universidade Estadual Paulista[a], Universidade Federal do ABC[b], São Paulo, Brazil

C.A. Bernardes[a], L. Calligaris[a], T.R. Fernandez Perez Tomei[a], E.M. Gregores[b], D.S. Lemos[a], P.G. Mercadante[b], S.F. Novaes[a], Sandra S. Padula[a]

2020 JINST 15 P10002

Institute for Nuclear Research and Nuclear Energy, Bulgarian Academy of Sciences, Sofia, Bulgaria

A. Aleksandrov, G. Antchev, I. Atanasov, R. Hadjiiska, P. Iaydjiev, M. Misheva, M. Rodozov, M. Shopova, G. Sultanov

University of Sofia, Sofia, Bulgaria

M. Bonchev, A. Dimitrov, T. Ivanov, L. Litov, B. Pavlov, P. Petkov, A. Petrov

Beihang University, Beijing, China

W. Fang[3], Q. Guo, H. Wang, L. Yuan

Department of Physics, Tsinghua University, Beijing, China

M. Ahmad, Z. Hu, Y. Wang

Institute of High Energy Physics, Beijing, China

E. Chapon, G.M. Chen[9], H.S. Chen[9], M. Chen, D. Leggat, H. Liao, Z. Liu, R. Sharma, A. Spiezia, J. Tao, J. Thomas-wilsker, J. Wang, H. Zhang, S. Zhang[9], J. Zhao

State Key Laboratory of Nuclear Physics and Technology, Peking University, Beijing, China

A. Agapitos, Y. Ban, C. Chen, A. Levin, J. Li, Q. Li, M. Lu, X. Lyu, Y. Mao, S.J. Qian, D. Wang, Q. Wang, J. Xiao

Sun Yat-Sen University, Guangzhou, China

Z. You

Institute of Modern Physics and Key Laboratory of Nuclear Physics and Ion-beam Application (MOE) — Fudan University, Shanghai, China

X. Gao[3]

Zhejiang University, Hangzhou, China

M. Xiao

Universidad de Los Andes, Bogota, Colombia

C. Avila, A. Cabrera, C. Florez, J. Fraga, A. Sarkar, M.A. Segura Delgado

Universidad de Antioquia, Medellin, Colombia

J. Jaramillo, J. Mejia Guisao, F. Ramirez, J.D. Ruiz Alvarez, C.A. Salazar González, N. Vanegas Arbelaez

University of Split, Faculty of Electrical Engineering, Mechanical Engineering and Naval Architecture, Split, Croatia

D. Giljanovic, N. Godinovic, D. Lelas, I. Puljak, T. Sculac

University of Split, Faculty of Science, Split, Croatia

Z. Antunovic, M. Kovac

Institute Rudjer Boskovic, Zagreb, Croatia

V. Brigljevic, D. Ferencek, D. Majumder, B. Mesic, M. Roguljic, A. Starodumov[10], T. Susa

2020 JINST 15 P10002

University of Cyprus, Nicosia, Cyprus
M.W. Ather, A. Attikis, E. Erodotou, A. Ioannou, G. Kole, M. Kolosova, S. Konstantinou, G. Mavromanolakis, J. Mousa, C. Nicolaou, F. Ptochos, P.A. Razis, H. Rykaczewski, H. Saka, D. Tsiakkouri

Charles University, Prague, Czech Republic
M. Finger[11], M. Finger Jr.[11], A. Kveton, J. Tomsa

Escuela Politecnica Nacional, Quito, Ecuador
E. Ayala

Universidad San Francisco de Quito, Quito, Ecuador
E. Carrera Jarrin

Academy of Scientific Research and Technology of the Arab Republic of Egypt, Egyptian Network of High Energy Physics, Cairo, Egypt
Y. Assran[12,13], A. Mohamed[14], E. Salama[13,15]

Center for High Energy Physics (CHEP-FU), Fayoum University, El-Fayoum, Egypt
M.A. Mahmoud, Y. Mohammed[16]

National Institute of Chemical Physics and Biophysics, Tallinn, Estonia
S. Bhowmik, A. Carvalho Antunes De Oliveira, R.K. Dewanjee, K. Ehataht, M. Kadastik, M. Raidal, C. Veelken

Department of Physics, University of Helsinki, Helsinki, Finland
P. Eerola, L. Forthomme, H. Kirschenmann, K. Osterberg, M. Voutilainen

Helsinki Institute of Physics, Helsinki, Finland
E. Brücken, F. Garcia, J. Havukainen, V. Karimäki, M.S. Kim, R. Kinnunen, T. Lampén, K. Lassila-Perini, S. Laurila, S. Lehti, T. Lindén, H. Siikonen, E. Tuominen, J. Tuominiemi

Lappeenranta University of Technology, Lappeenranta, Finland
P. Luukka, T. Tuuva

IRFU, CEA, Université Paris-Saclay, Gif-sur-Yvette, France
C. Amendola, M. Besancon, F. Couderc, M. Dejardin, D. Denegri, J.L. Faure, F. Ferri, S. Ganjour, A. Givernaud, P. Gras, G. Hamel de Monchenault, P. Jarry, B. Lenzi, E. Locci, J. Malcles, J. Rander, A. Rosowsky, M.Ö. Sahin, A. Savoy-Navarro[17], M. Titov, G.B. Yu

Laboratoire Leprince-Ringuet, CNRS/IN2P3, Ecole Polytechnique, Institut Polytechnique de Paris, Paris, France
S. Ahuja, F. Beaudette, M. Bonanomi, A. Buchot Perraguin, P. Busson, C. Charlot, O. Davignon, B. Diab, G. Falmagne, R. Granier de Cassagnac, A. Hakimi, I. Kucher, A. Lobanov, C. Martin Perez, M. Nguyen, C. Ochando, P. Paganini, J. Rembser, R. Salerno, J.B. Sauvan, Y. Sirois, A. Zabi, A. Zghiche

Université de Strasbourg, CNRS, IPHC UMR 7178, Strasbourg, France
J.-L. Agram[18], J. Andrea, D. Bloch, G. Bourgatte, J.-M. Brom, E.C. Chabert, C. Collard, J.-C. Fontaine[18], D. Gelé, U. Goerlach, C. Grimault, A.-C. Le Bihan, P. Van Hove

2020 JINST 15 P10002

Université de Lyon, Université Claude Bernard Lyon 1, CNRS-IN2P3, Institut de Physique Nucléaire de Lyon, Villeurbanne, France

E. Asilar, S. Beauceron, C. Bernet, G. Boudoul, C. Camen, A. Carle, N. Chanon, D. Contardo, P. Depasse, H. El Mamouni, J. Fay, S. Gascon, M. Gouzevitch, B. Ille, Sa. Jain, I.B. Laktineh, H. Lattaud, A. Lesauvage, M. Lethuillier, L. Mirabito, L. Torterotot, G. Touquet, M. Vander Donckt, S. Viret

Georgian Technical University, Tbilisi, Georgia

G. Adamov, Z. Tsamalaidze[11]

RWTH Aachen University, I. Physikalisches Institut, Aachen, Germany

L. Feld, K. Klein, M. Lipinski, D. Meuser, A. Pauls, M. Preuten, M.P. Rauch, J. Schulz, M. Teroerde

RWTH Aachen University, III. Physikalisches Institut A, Aachen, Germany

D. Eliseev, M. Erdmann, P. Fackeldey, B. Fischer, S. Ghosh, T. Hebbeker, K. Hoepfner, H. Keller, L. Mastrolorenzo, M. Merschmeyer, A. Meyer, P. Millet, G. Mocellin, S. Mondal, S. Mukherjee, D. Noll, A. Novak, T. Pook, A. Pozdnyakov, T. Quast, M. Radziej, Y. Rath, H. Reithler, J. Roemer, A. Schmidt, S.C. Schuler, A. Sharma, S. Wiedenbeck, S. Zaleski

RWTH Aachen University, III. Physikalisches Institut B, Aachen, Germany

C. Dziwok, G. Flügge, W. Haj Ahmad[19], O. Hlushchenko, T. Kress, A. Nowack, C. Pistone, O. Pooth, D. Roy, H. Sert, A. Stahl[20], T. Ziemons

Deutsches Elektronen-Synchrotron, Hamburg, Germany

H. Aarup Petersen, M. Aldaya Martin, P. Asmuss, I. Babounikau, S. Baxter, O. Behnke, A. Bermúdez Martínez, A.A. Bin Anuar, K. Borras[21], V. Botta, D. Brunner, A. Campbell, A. Cardini, P. Connor, S. Consuegra Rodríguez, V. Danilov, A. De Wit, M.M. Defranchis, L. Didukh, D. Domínguez Damiani, G. Eckerlin, D. Eckstein, T. Eichhorn, A. Elwood, L.I. Estevez Banos, E. Gallo[22], A. Geiser, A. Giraldi, A. Grohsjean, M. Guthoff, A. Harb, A. Jafari[23], N.Z. Jomhari, H. Jung, A. Kasem[21], M. Kasemann, H. Kaveh, C. Kleinwort, J. Knolle, D. Krücker, W. Lange, T. Lenz, J. Lidrych, K. Lipka, W. Lohmann[24], R. Mankel, I.-A. Melzer-Pellmann, J. Metwally, A.B. Meyer, M. Meyer, M. Missiroli, J. Mnich, A. Mussgiller, V. Myronenko, Y. Otarid, D. Pérez Adán, S.K. Pflitsch, D. Pitzl, A. Raspereza, A. Saggio, A. Saibel, M. Savitskyi, V. Scheurer, P. Schütze, C. Schwanenberger, R. Shevchenko, A. Singh, R.E. Sosa Ricardo, H. Tholen, N. Tonon, O. Turkot, A. Vagnerini, M. Van De Klundert, R. Walsh, D. Walter, Y. Wen, K. Wichmann, C. Wissing, S. Wuchterl, O. Zenaiev, R. Zlebcik

University of Hamburg, Hamburg, Germany

R. Aggleton, S. Bein, L. Benato, A. Benecke, K. De Leo, T. Dreyer, A. Ebrahimi, F. Feindt, A. Fröhlich, C. Garbers, E. Garutti, P. Gunnellini, J. Haller, A. Hinzmann, A. Karavdina, G. Kasieczka, R. Klanner, R. Kogler, V. Kutzner, J. Lange, T. Lange, A. Malara, J. Multhaup, C.E.N. Niemeyer, A. Nigamova, K.J. Pena Rodriguez, O. Rieger, P. Schleper, S. Schumann, J. Schwandt, D. Schwarz, J. Sonneveld, H. Stadie, G. Steinbrück, B. Vormwald, I. Zoi

Karlsruher Institut fuer Technologie, Karlsruhe, Germany

M. Baselga, S. Baur, J. Bechtel, T. Berger, E. Butz, R. Caspart, T. Chwalek, W. De Boer, A. Dierlamm, A. Droll, K. El Morabit, N. Faltermann, K. Flöh, M. Giffels, A. Gottmann,

2020 JINST 15 P10002

F. Hartmann[20], C. Heidecker, U. Husemann, M.A. Iqbal, I. Katkov[25], P. Keicher, R. Koppenhöfer, S. Maier, M. Metzler, S. Mitra, M.U. Mozer, D. Müller, Th. Müller, M. Musich, G. Quast, K. Rabbertz, J. Rauser, D. Savoiu, D. Schäfer, M. Schnepf, M. Schröder, D. Seith, I. Shvetsov, H.J. Simonis, R. Ulrich, M. Wassmer, M. Weber, C. Wöhrmann, R. Wolf, S. Wozniewski

Institute of Nuclear and Particle Physics (INPP), NCSR Demokritos, Aghia Paraskevi, Greece
G. Anagnostou, P. Asenov, G. Daskalakis, T. Geralis, A. Kyriakis, D. Loukas, G. Paspalaki, A. Stakia

National and Kapodistrian University of Athens, Athens, Greece
M. Diamantopoulou, D. Karasavvas, G. Karathanasis, P. Kontaxakis, C.K. Koraka, A. Manousakis-katsikakis, A. Panagiotou, I. Papavergou, N. Saoulidou, K. Theofilatos, K. Vellidis, E. Vourliotis

National Technical University of Athens, Athens, Greece
G. Bakas, K. Kousouris, I. Papakrivopoulos, G. Tsipolitis, A. Zacharopoulou

University of Ioánnina, Ioánnina, Greece
I. Evangelou, C. Foudas, P. Gianneios, P. Katsoulis, P. Kokkas, S. Mallios, K. Manitara, N. Manthos, I. Papadopoulos, J. Strologas

MTA-ELTE Lendület CMS Particle and Nuclear Physics Group, Eötvös Loránd University, Budapest, Hungary
M. Bartók[26], R. Chudasama, M. Csanad, M.M.A. Gadallah[27], S. Lökös[28], P. Major, K. Mandal, A. Mehta, G. Pasztor, O. Surányi, G.I. Veres

Wigner Research Centre for Physics, Budapest, Hungary
G. Bencze, C. Hajdu, D. Horvath[29], F. Sikler, V. Veszpremi, G. Vesztergombi[†]

Institute of Nuclear Research ATOMKI, Debrecen, Hungary
S. Czellar, J. Karancsi[26], J. Molnar, Z. Szillasi, D. Teyssier

Institute of Physics, University of Debrecen, Debrecen, Hungary
P. Raics, Z.L. Trocsanyi, B. Ujvari

Eszterhazy Karoly University, Karoly Robert Campus, Gyongyos, Hungary
T. Csorgo, F. Nemes, T. Novak

Indian Institute of Science (IISc), Bangalore, India
S. Choudhury, J.R. Komaragiri, D. Kumar, L. Panwar, P.C. Tiwari

National Institute of Science Education and Research, HBNI, Bhubaneswar, India
S. Bahinipati[30], D. Dash, C. Kar, P. Mal, T. Mishra, V.K. Muraleedharan Nair Bindhu, A. Nayak[31], D.K. Sahoo[30], N. Sur, S.K. Swain

Panjab University, Chandigarh, India
S. Bansal, S.B. Beri, V. Bhatnagar, S. Chauhan, N. Dhingra[32], R. Gupta, A. Kaur, S. Kaur, P. Kumari, M. Lohan, M. Meena, K. Sandeep, S. Sharma, J.B. Singh, A.K. Virdi

University of Delhi, Delhi, India
A. Ahmed, A. Bhardwaj, B.C. Choudhary, R.B. Garg, M. Gola, S. Keshri, A. Kumar, M. Naimuddin, P. Priyanka, K. Ranjan, A. Shah

2020 JINST 15 P10002

Saha Institute of Nuclear Physics, HBNI, Kolkata, India

M. Bharti[33], R. Bhattacharya, S. Bhattacharya, D. Bhowmik, S. Dutta, S. Ghosh, B. Gomber[34], M. Maity[35], S. Nandan, P. Palit, A. Purohit, P.K. Rout, G. Saha, S. Sarkar, M. Sharan, B. Singh[33], S. Thakur[33]

Indian Institute of Technology Madras, Madras, India

P.K. Behera, S.C. Behera, P. Kalbhor, A. Muhammad, R. Pradhan, P.R. Pujahari, A. Sharma, A.K. Sikdar

Bhabha Atomic Research Centre, Mumbai, India

D. Dutta, V. Jha, V. Kumar, D.K. Mishra, K. Naskar[36], P.K. Netrakanti, L.M. Pant, P. Shukla

Tata Institute of Fundamental Research-A, Mumbai, India

T. Aziz, M.A. Bhat, S. Dugad, R. Kumar Verma, U. Sarkar

Tata Institute of Fundamental Research-B, Mumbai, India

S. Banerjee, S. Bhattacharya, S. Chatterjee, P. Das, M. Guchait, S. Karmakar, S. Kumar, G. Majumder, K. Mazumdar, S. Mukherjee, D. Roy, N. Sahoo

Indian Institute of Science Education and Research (IISER), Pune, India

S. Dube, B. Kansal, A. Kapoor, K. Kothekar, S. Pandey, A. Rane, A. Rastogi, S. Sharma

Department of Physics, Isfahan University of Technology, Isfahan, Iran

H. Bakhshiansohi[37]

Institute for Research in Fundamental Sciences (IPM), Tehran, Iran

S. Chenarani[38], S.M. Etesami, M. Khakzad, M. Mohammadi Najafabadi

University College Dublin, Dublin, Ireland

M. Felcini, M. Grunewald

INFN Sezione di Bari[a], Università di Bari[b], Politecnico di Bari[c], Bari, Italy

M. Abbrescia[a,b], R. Aly[a,b,39], C. Aruta[a,b], A. Colaleo[a], D. Creanza[a,c], N. De Filippis[a,c], M. De Palma[a,b], A. Di Florio[a,b], A. Di Pilato[a,b], W. Elmetenawee[a,b], L. Fiore[a], A. Gelmi[a,b], M. Gul[a], G. Iaselli[a,c], M. Ince[a,b], S. Lezki[a,b], G. Maggi[a,c], M. Maggi[a], I. Margjeka[a,b], J.A. Merlin[a], S. My[a,b], S. Nuzzo[a,b], A. Pompili[a,b], G. Pugliese[a,c], A. Ranieri[a], G. Selvaggi[a,b], L. Silvestris[a], F.M. Simone[a,b], R. Venditti[a], P. Verwilligen[a]

INFN Sezione di Bologna[a], Università di Bologna[b], Bologna, Italy

G. Abbiendi[a], C. Battilana[a,b], D. Bonacorsi[a,b], L. Borgonovi[a,b], S. Braibant-Giacomelli[a,b], R. Campanini[a,b], P. Capiluppi[a,b], A. Castro[a,b], F.R. Cavallo[a], C. Ciocca[a], M. Cuffiani[a,b], G.M. Dallavalle[a], T. Diotalevi[a,b], F. Fabbri[a], A. Fanfani[a,b], E. Fontanesi[a,b], P. Giacomelli[a], C. Grandi[a], L. Guiducci[a,b], F. Iemmi[a,b], S. Lo Meo[a,40], S. Marcellini[a], G. Masetti[a], F.L. Navarria[a,b], A. Perrotta[a], F. Primavera[a,b], A.M. Rossi[a,b], T. Rovelli[a,b], G.P. Siroli[a,b], N. Tosi[a]

INFN Sezione di Catania[a], Università di Catania[b], Catania, Italy

S. Albergo[a,b,41], S. Costa[a,b], A. Di Mattia[a], R. Potenza[a,b], A. Tricomi[a,b,41], C. Tuve[a,b]

2020 JINST 15 P10002

INFN Sezione di Firenze[a], Università di Firenze[b], Firenze, Italy
G. Barbagli[a], A. Cassese[a], R. Ceccarelli[a,b], V. Ciulli[a,b], C. Civinini[a], R. D'Alessandro[a,b], F. Fiori[a], E. Focardi[a,b], G. Latino[a,b], P. Lenzi[a,b], M. Lizzo[a,b], M. Meschini[a], S. Paoletti[a], R. Seidita[a,b], G. Sguazzoni[a], L. Viliani[a]

INFN Laboratori Nazionali di Frascati, Frascati, Italy
L. Benussi, S. Bianco, D. Piccolo

INFN Sezione di Genova[a], Università di Genova[b], Genova, Italy
M. Bozzo[a,b], F. Ferro[a], R. Mulargia[a,b], E. Robutti[a], S. Tosi[a,b]

INFN Sezione di Milano-Bicocca[a], Università di Milano-Bicocca[b], Milano, Italy
A. Benaglia[a], A. Beschi[a,b], F. Brivio[a,b], F. Cetorelli[a,b], V. Ciriolo[a,b,20], F. De Guio[a,b], M.E. Dinardo[a,b], P. Dini[a], S. Gennai[a], A. Ghezzi[a,b], P. Govoni[a,b], L. Guzzi[a,b], M. Malberti[a], S. Malvezzi[a], D. Menasce[a], F. Monti[a,b], L. Moroni[a], M. Paganoni[a,b], D. Pedrini[a], S. Ragazzi[a,b], T. Tabarelli de Fatis[a,b], D. Valsecchi[a,b,20], D. Zuolo[a,b]

INFN Sezione di Napoli[a], Università di Napoli 'Federico II'[b], Napoli, Italy, Università della Basilicata[c], Potenza, Italy, Università G. Marconi[d], Roma, Italy
S. Buontempo[a], N. Cavallo[a,c], A. De Iorio[a,b], F. Fabozzi[a,c], F. Fienga[a], A.O.M. Iorio[a,b], L. Layer[a,b], L. Lista[a,b], S. Meola[a,d,20], P. Paolucci[a,20], B. Rossi[a], C. Sciacca[a,b], E. Voevodina[a,b]

INFN Sezione di Padova[a], Università di Padova[b], Padova, Italy, Università di Trento[c], Trento, Italy
P. Azzi[a], N. Bacchetta[a], D. Bisello[a,b], A. Boletti[a,b], A. Bragagnolo[a,b], R. Carlin[a,b], P. De Castro Manzano[a], T. Dorigo[a], F. Gasparini[a,b], U. Gasparini[a,b], S.Y. Hoh[a,b], M. Margoni[a,b], A.T. Meneguzzo[a,b], M. Presilla[b], P. Ronchese[a,b], R. Rossin[a,b], F. Simonetto[a,b], G. Strong, A. Tiko[a], M. Tosi[a,b], H. YARAR[a,b], M. Zanetti[a,b], P. Zotto[a,b], A. Zucchetta[a,b], G. Zumerle[a,b]

INFN Sezione di Pavia[a], Università di Pavia[b], Pavia, Italy
A. Braghieri[a], S. Calzaferri[a,b], D. Fiorina[a,b], P. Montagna[a,b], S.P. Ratti[a,b], V. Re[a], M. Ressegotti[a,b], C. Riccardi[a,b], P. Salvini[a], I. Vai[a], P. Vitulo[a,b]

INFN Sezione di Perugia[a], Università di Perugia[b], Perugia, Italy
M. Biasini[a,b], G.M. Bilei[a], D. Ciangottini[a,b], L. Fanò[a,b], P. Lariccia[a,b], G. Mantovani[a,b], V. Mariani[a,b], M. Menichelli[a], F. Moscatelli[a], A. Rossi[a,b], A. Santocchia[a,b], D. Spiga[a], T. Tedeschi[a,b]

INFN Sezione di Pisa[a], Università di Pisa[b], Scuola Normale Superiore di Pisa[c], Pisa, Italy
K. Androsov[a], P. Azzurri[a], G. Bagliesi[a], V. Bertacchi[a,c], L. Bianchini[a], T. Boccali[a], R. Castaldi[a], M.A. Ciocci[a,b], R. Dell'Orso[a], M.R. Di Domenico[a,b], S. Donato[a], L. Giannini[a,c], A. Giassi[a], M.T. Grippo[a], F. Ligabue[a,c], E. Manca[a,c], G. Mandorli[a,c], A. Messineo[a,b], F. Palla[a], G. Ramirez-Sanchez[a,c], A. Rizzi[a,b], G. Rolandi[a,c], S. Roy Chowdhury[a,c], A. Scribano[a], N. Shafiei[a,b], P. Spagnolo[a], R. Tenchini[a], G. Tonelli[a,b], N. Turini[a], A. Venturi[a], P.G. Verdini[a]

INFN Sezione di Roma[a], Sapienza Università di Roma[b], Rome, Italy
F. Cavallari[a], M. Cipriani[a,b], D. Del Re[a,b], E. Di Marco[a], M. Diemoz[a], E. Longo[a,b], P. Meridiani[a], G. Organtini[a,b], F. Pandolfi[a], R. Paramatti[a,b], C. Quaranta[a,b], S. Rahatlou[a,b], C. Rovelli[a], F. Santanastasio[a,b], L. Soffi[a,b], R. Tramontano[a,b]

2020 JINST 15 P10002

INFN Sezione di Torino[a], Università di Torino[b], Torino, Italy, Università del Piemonte Orientale[c], Novara, Italy

N. Amapane[a,b], R. Arcidiacono[a,c], S. Argiro[a,b], M. Arneodo[a,c], N. Bartosik[a], R. Bellan[a,b], A. Bellora[a,b], C. Biino[a], A. Cappati[a,b], N. Cartiglia[a], S. Cometti[a], M. Costa[a,b], R. Covarelli[a,b], N. Demaria[a], B. Kiani[a,b], F. Legger[a], C. Mariotti[a], S. Maselli[a], E. Migliore[a,b], V. Monaco[a,b], E. Monteil[a,b], M. Monteno[a], M.M. Obertino[a,b], G. Ortona[a], L. Pacher[a,b], N. Pastrone[a], M. Pelliccioni[a], G.L. Pinna Angioni[a,b], M. Ruspa[a,c], R. Salvatico[a,b], F. Siviero[a,b], V. Sola[a], A. Solano[a,b], D. Soldi[a,b], A. Staiano[a], D. Trocino[a,b]

INFN Sezione di Trieste[a], Università di Trieste[b], Trieste, Italy

S. Belforte[a], V. Candelise[a,b], M. Casarsa[a], F. Cossutti[a], A. Da Rold[a,b], G. Della Ricca[a,b], F. Vazzoler[a,b]

Kyungpook National University, Daegu, Korea

S. Dogra, C. Huh, B. Kim, D.H. Kim, G.N. Kim, J. Lee, S.W. Lee, C.S. Moon, Y.D. Oh, S.I. Pak, S. Sekmen, Y.C. Yang

Chonnam National University, Institute for Universe and Elementary Particles, Kwangju, Korea

H. Kim, D.H. Moon

Hanyang University, Seoul, Korea

B. Francois, T.J. Kim, J. Park

Korea University, Seoul, Korea

S. Cho, S. Choi, Y. Go, S. Ha, B. Hong, K. Lee, K.S. Lee, J. Lim, J. Park, S.K. Park, J. Yoo

Kyung Hee University, Department of Physics, Seoul, Republic of Korea

J. Goh, A. Gurtu

Sejong University, Seoul, Korea

H.S. Kim, Y. Kim

Seoul National University, Seoul, Korea

J. Almond, J.H. Bhyun, J. Choi, S. Jeon, J. Kim, J.S. Kim, S. Ko, H. Kwon, H. Lee, K. Lee, S. Lee, K. Nam, B.H. Oh, M. Oh, S.B. Oh, B.C. Radburn-Smith, H. Seo, U.K. Yang, I. Yoon

University of Seoul, Seoul, Korea

D. Jeon, J.H. Kim, B. Ko, J.S.H. Lee, I.C. Park, Y. Roh, D. Song, I.J. Watson

Yonsei University, Department of Physics, Seoul, Korea

H.D. Yoo

Sungkyunkwan University, Suwon, Korea

Y. Choi, C. Hwang, Y. Jeong, H. Lee, Y. Lee, I. Yu

Riga Technical University, Riga, Latvia

V. Veckalns[42]

2020 JINST 15 P10002

Vilnius University, Vilnius, Lithuania
A. Juodagalvis, A. Rinkevicius, G. Tamulaitis

National Centre for Particle Physics, Universiti Malaya, Kuala Lumpur, Malaysia
W.A.T. Wan Abdullah, M.N. Yusli, Z. Zolkapli

Universidad de Sonora (UNISON), Hermosillo, Mexico
J.F. Benitez, A. Castaneda Hernandez, J.A. Murillo Quijada, L. Valencia Palomo

Centro de Investigacion y de Estudios Avanzados del IPN, Mexico City, Mexico
H. Castilla-Valdez, E. De La Cruz-Burelo, I. Heredia-De La Cruz[43], R. Lopez-Fernandez, A. Sanchez-Hernandez

Universidad Iberoamericana, Mexico City, Mexico
S. Carrillo Moreno, C. Oropeza Barrera, M. Ramirez-Garcia, F. Vazquez Valencia

Benemerita Universidad Autonoma de Puebla, Puebla, Mexico
J. Eysermans, I. Pedraza, H.A. Salazar Ibarguen, C. Uribe Estrada

Universidad Autónoma de San Luis Potosí, San Luis Potosí, Mexico
A. Morelos Pineda

University of Montenegro, Podgorica, Montenegro
J. Mijuskovic[4], N. Raicevic

University of Auckland, Auckland, New Zealand
D. Krofcheck

University of Canterbury, Christchurch, New Zealand
S. Bheesette, P.H. Butler

National Centre for Physics, Quaid-I-Azam University, Islamabad, Pakistan
A. Ahmad, M.I. Asghar, M.I.M. Awan, Q. Hassan, H.R. Hoorani, W.A. Khan, M.A. Shah, M. Shoaib, M. Waqas

AGH University of Science and Technology Faculty of Computer Science, Electronics and Telecommunications, Krakow, Poland
V. Avati, L. Grzanka, M. Malawski

National Centre for Nuclear Research, Swierk, Poland
H. Bialkowska, M. Bluj, B. Boimska, T. Frueboes, M. Górski, M. Kazana, M. Szleper, P. Traczyk, P. Zalewski

Institute of Experimental Physics, Faculty of Physics, University of Warsaw, Warsaw, Poland
K. Bunkowski, A. Byszuk[44], K. Doroba, A. Kalinowski, M. Konecki, J. Krolikowski, M. Olszewski, M. Walczak

Laboratório de Instrumentação e Física Experimental de Partículas, Lisboa, Portugal
M. Araujo, P. Bargassa, D. Bastos, P. Faccioli, M. Gallinaro, J. Hollar, N. Leonardo, T. Niknejad, J. Seixas, K. Shchelina, O. Toldaiev, J. Varela

2020 JINST 15 P10002

Joint Institute for Nuclear Research, Dubna, Russia

S. Afanasiev, P. Bunin, M. Gavrilenko, I. Golutvin, I. Gorbunov, A. Kamenev, V. Karjavine, A. Lanev, A. Malakhov, V. Matveev[45,46], P. Moisenz, V. Palichik, V. Perelygin, M. Savina, D. Seitova, V. Shalaev, S. Shmatov, S. Shulha, V. Smirnov, O. Teryaev, N. Voytishin, A. Zarubin, I. Zhizhin

Petersburg Nuclear Physics Institute, Gatchina (St. Petersburg), Russia

G. Gavrilov, V. Golovtcov, Y. Ivanov, V. Kim[47], E. Kuznetsova[48], V. Murzin, V. Oreshkin, I. Smirnov, D. Sosnov, V. Sulimov, L. Uvarov, S. Volkov, A. Vorobyev

Institute for Nuclear Research, Moscow, Russia

Yu. Andreev, A. Dermenev, S. Gninenko, N. Golubev, A. Karneyeu, M. Kirsanov, N. Krasnikov, A. Pashenkov, G. Pivovarov, D. Tlisov, A. Toropin

Institute for Theoretical and Experimental Physics named by A.I. Alikhanov of NRC 'Kurchatov Institute', Moscow, Russia

V. Epshteyn, V. Gavrilov, N. Lychkovskaya, A. Nikitenko[49], V. Popov, I. Pozdnyakov, G. Safronov, A. Spiridonov, A. Stepennov, M. Toms, E. Vlasov, A. Zhokin

Moscow Institute of Physics and Technology, Moscow, Russia

T. Aushev

National Research Nuclear University 'Moscow Engineering Physics Institute' (MEPhI), Moscow, Russia

M. Danilov[50], P. Parygin, D. Philippov, E. Popova, V. Rusinov

P.N. Lebedev Physical Institute, Moscow, Russia

V. Andreev, M. Azarkin, I. Dremin, M. Kirakosyan, A. Terkulov

Skobeltsyn Institute of Nuclear Physics, Lomonosov Moscow State University, Moscow, Russia

A. Belyaev, E. Boos, A. Demiyanov, A. Ershov, A. Gribushin, A. Kaminskiy[51], V. Klyukhin, O. Kodolova, I. Lokhtin, S. Obraztsov, S. Petrushanko, V. Savrin, A. Snigirev

Novosibirsk State University (NSU), Novosibirsk, Russia

V. Blinov[52], T. Dimova[52], L. Kardapoltsev[52], I. Ovtin[52], Y. Skovpen[52]

Institute for High Energy Physics of National Research Centre 'Kurchatov Institute', Protvino, Russia

I. Azhgirey, I. Bayshev, V. Kachanov, A. Kalinin, D. Konstantinov, V. Petrov, R. Ryutin, A. Sobol, S. Troshin, N. Tyurin, A. Uzunian, A. Volkov

National Research Tomsk Polytechnic University, Tomsk, Russia

A. Babaev, A. Iuzhakov, V. Okhotnikov, L. Sukhikh

Tomsk State University, Tomsk, Russia

V. Borchsh, V. Ivanchenko, E. Tcherniaev

University of Belgrade: Faculty of Physics and VINCA Institute of Nuclear Sciences, Belgrade, Serbia

P. Adzic[53], P. Cirkovic, M. Dordevic, P. Milenovic, J. Milosevic

2020 JINST 15 P10002

Centro de Investigaciones Energéticas Medioambientales y Tecnológicas (CIEMAT), Madrid, Spain

M. Aguilar-Benitez, J. Alcaraz Maestre, A. Álvarez Fernández, I. Bachiller, M. Barrio Luna, Cristina F. Bedoya, J.A. Brochero Cifuentes, C.A. Carrillo Montoya, M. Cepeda, M. Cerrada, N. Colino, B. De La Cruz, A. Delgado Peris, J.P. Fernández Ramos, J. Flix, M.C. Fouz, A. García Alonso, O. Gonzalez Lopez, S. Goy Lopez, J.M. Hernandez, M.I. Josa, J. León Holgado, D. Moran, Á. Navarro Tobar, A. Pérez-Calero Yzquierdo, J. Puerta Pelayo, I. Redondo, L. Romero, S. Sánchez Navas, M.S. Soares, A. Triossi, C. Willmott

Universidad Autónoma de Madrid, Madrid, Spain

C. Albajar, J.F. de Trocóniz, R. Reyes-Almanza

Universidad de Oviedo, Instituto Universitario de Ciencias y Tecnologías Espaciales de Asturias (ICTEA), Oviedo, Spain

B. Alvarez Gonzalez, J. Cuevas, C. Erice, J. Fernandez Menendez, S. Folgueras, I. Gonzalez Caballero, E. Palencia Cortezon, C. Ramón Álvarez, J. Ripoll Sau, V. Rodríguez Bouza, S. Sanchez Cruz, A. Trapote

Instituto de Física de Cantabria (IFCA), CSIC-Universidad de Cantabria, Santander, Spain

I.J. Cabrillo, A. Calderon, B. Chazin Quero, J. Duarte Campderros, M. Fernandez, P.J. Fernández Manteca, G. Gomez, C. Martinez Rivero, P. Martinez Ruiz del Arbol, F. Matorras, J. Piedra Gomez, C. Prieels, F. Ricci-Tam, T. Rodrigo, A. Ruiz-Jimeno, L. Russo[54], L. Scodellaro, I. Vila, J.M. Vizan Garcia

University of Colombo, Colombo, Sri Lanka

MK Jayananda, B. Kailasapathy[55], D.U.J. Sonnadara, DDC Wickramarathna

University of Ruhuna, Department of Physics, Matara, Sri Lanka

W.G.D. Dharmaratna, K. Liyanage, N. Perera, N. Wickramage

CERN, European Organization for Nuclear Research, Geneva, Switzerland

T.K. Aarrestad, D. Abbaneo, B. Akgun, E. Auffray, G. Auzinger, J. Baechler, P. Baillon, A.H. Ball, D. Barney, J. Bendavid, N. Beni, M. Bianco, A. Bocci, P. Bortignon, E. Bossini, E. Brondolin, T. Camporesi, G. Cerminara, L. Cristella, D. d'Enterria, A. Dabrowski, N. Daci, V. Daponte, A. David, A. De Roeck, M. Deile, R. Di Maria, M. Dobson, M. Dünser, N. Dupont, A. Elliott-Peisert, N. Emriskova, F. Fallavollita[56], D. Fasanella, S. Fiorendi, G. Franzoni, J. Fulcher, W. Funk, S. Giani, D. Gigi, K. Gill, F. Glege, L. Gouskos, M. Guilbaud, D. Gulhan, M. Haranko, J. Hegeman, Y. Iiyama, V. Innocente, T. James, P. Janot, J. Kaspar, J. Kieseler, M. Komm, N. Kratochwil, C. Lange, P. Lecoq, K. Long, C. Lourenço, L. Malgeri, M. Mannelli, A. Massironi, F. Meijers, S. Mersi, E. Meschi, F. Moortgat, M. Mulders, J. Ngadiuba, J. Niedziela, S. Orfanelli, L. Orsini, F. Pantaleo[20], L. Pape, E. Perez, M. Peruzzi, A. Petrilli, G. Petrucciani, A. Pfeiffer, M. Pierini, D. Rabady, A. Racz, M. Rieger, M. Rovere, H. Sakulin, J. Salfeld-Nebgen, S. Scarfi, C. Schäfer, C. Schwick, M. Selvaggi, A. Sharma, P. Silva, W. Snoeys, P. Sphicas[57], J. Steggemann, S. Summers, V.R. Tavolaro, D. Treille, A. Tsirou, G.P. Van Onsem, A. Vartak, M. Verzetti, K.A. Wozniak, W.D. Zeuner

2020 JINST 15 P10002

Paul Scherrer Institut, Villigen, Switzerland
L. Caminada[58], W. Erdmann, R. Horisberger, Q. Ingram, H.C. Kaestli, D. Kotlinski, U. Langenegger, T. Rohe

ETH Zurich — Institute for Particle Physics and Astrophysics (IPA), Zurich, Switzerland
M. Backhaus, P. Berger, A. Calandri, N. Chernyavskaya, G. Dissertori, M. Dittmar, M. Donegà, C. Dorfer, T. Gadek, T.A. Gómez Espinosa, C. Grab, D. Hits, W. Lustermann, A.-M. Lyon, R.A. Manzoni, M.T. Meinhard, F. Micheli, F. Nessi-Tedaldi, F. Pauss, V. Perovic, G. Perrin, L. Perrozzi, S. Pigazzini, M.G. Ratti, M. Reichmann, C. Reissel, T. Reitenspiess, B. Ristic, D. Ruini, D.A. Sanz Becerra, M. Schönenberger, L. Shchutska, V. Stampf, M.L. Vesterbacka Olsson, R. Wallny, D.H. Zhu

Universität Zürich, Zurich, Switzerland
C. Amsler[59], C. Botta, D. Brzhechko, M.F. Canelli, A. De Cosa, R. Del Burgo, J.K. Heikkilä, M. Huwiler, A. Jofrehei, B. Kilminster, S. Leontsinis, A. Macchiolo, P. Meiring, V.M. Mikuni, U. Molinatti, I. Neutelings, G. Rauco, A. Reimers, P. Robmann, K. Schweiger, Y. Takahashi, S. Wertz

National Central University, Chung-Li, Taiwan
C. Adloff[60], C.M. Kuo, W. Lin, A. Roy, T. Sarkar[35], S.S. Yu

National Taiwan University (NTU), Taipei, Taiwan
L. Ceard, P. Chang, Y. Chao, K.F. Chen, P.H. Chen, W.-S. Hou, Y.y. Li, R.-S. Lu, E. Paganis, A. Psallidas, A. Steen, E. Yazgan

Chulalongkorn University, Faculty of Science, Department of Physics, Bangkok, Thailand
B. Asavapibhop, C. Asawatangtrakuldee, N. Srimanobhas

Çukurova University, Physics Department, Science and Art Faculty, Adana, Turkey
F. Boran, S. Damarseckin[61], Z.S. Demiroglu, F. Dolek, C. Dozen[62], I. Dumanoglu[63], E. Eskut, G. Gokbulut, Y. Guler, E. Gurpinar Guler[64], I. Hos[65], C. Isik, E.E. Kangal[66], O. Kara, A. Kayis Topaksu, U. Kiminsu, G. Onengut, K. Ozdemir[67], A. Polatoz, A.E. Simsek, B. Tali[68], U.G. Tok, S. Turkcapar, I.S. Zorbakir, C. Zorbilmez

Middle East Technical University, Physics Department, Ankara, Turkey
B. Isildak[69], G. Karapinar[70], K. Ocalan[71], M. Yalvac[72]

Bogazici University, Istanbul, Turkey
I.O. Atakisi, E. Gülmez, M. Kaya[73], O. Kaya[74], Ö. Özçelik, S. Tekten[75], E.A. Yetkin[76]

Istanbul Technical University, Istanbul, Turkey
A. Cakir, K. Cankocak[63], Y. Komurcu, S. Sen[77]

Istanbul University, Istanbul, Turkey
F. Aydogmus Sen, S. Cerci[68], B. Kaynak, S. Ozkorucuklu, D. Sunar Cerci[68]

Institute for Scintillation Materials of National Academy of Science of Ukraine, Kharkov, Ukraine
B. Grynyov

2020 JINST 15 P10002

National Scientific Center, Kharkov Institute of Physics and Technology, Kharkov, Ukraine
L. Levchuk

University of Bristol, Bristol, United Kingdom
E. Bhal, S. Bologna, J.J. Brooke, E. Clement, D. Cussans, H. Flacher, J. Goldstein, G.P. Heath, H.F. Heath, L. Kreczko, B. Krikler, S. Paramesvaran, T. Sakuma, S. Seif El Nasr-Storey, V.J. Smith, J. Taylor, A. Titterton

Rutherford Appleton Laboratory, Didcot, United Kingdom
K.W. Bell, A. Belyaev[78], C. Brew, R.M. Brown, D.J.A. Cockerill, K.V. Ellis, K. Harder, S. Harper, J. Linacre, K. Manolopoulos, D.M. Newbold, E. Olaiya, D. Petyt, T. Reis, T. Schuh, C.H. Shepherd-Themistocleous, A. Thea, I.R. Tomalin, T. Williams

Imperial College, London, United Kingdom
R. Bainbridge, P. Bloch, S. Bonomally, J. Borg, S. Breeze, O. Buchmuller, A. Bundock, V. Cepaitis, G.S. Chahal[79], D. Colling, P. Dauncey, G. Davies, M. Della Negra, P. Everaerts, G. Fedi, G. Hall, G. Iles, J. Langford, L. Lyons, A.-M. Magnan, S. Malik, A. Martelli, V. Milosevic, J. Nash[80], V. Palladino, M. Pesaresi, D.M. Raymond, A. Richards, A. Rose, E. Scott, C. Seez, A. Shtipliyski, M. Stoye, A. Tapper, K. Uchida, T. Virdee[20], N. Wardle, S.N. Webb, D. Winterbottom, A.G. Zecchinelli, S.C. Zenz

Brunel University, Uxbridge, United Kingdom
J.E. Cole, P.R. Hobson, A. Khan, P. Kyberd, C.K. Mackay, I.D. Reid, L. Teodorescu, S. Zahid

Baylor University, Waco, U.S.A.
A. Brinkerhoff, K. Call, B. Caraway, J. Dittmann, K. Hatakeyama, A.R. Kanuganti, C. Madrid, B. McMaster, N. Pastika, S. Sawant, C. Smith

Catholic University of America, Washington, DC, U.S.A.
R. Bartek, A. Dominguez, R. Uniyal, A.M. Vargas Hernandez

The University of Alabama, Tuscaloosa, U.S.A.
A. Buccilli, O. Charaf, S.I. Cooper, S.V. Gleyzer, C. Henderson, P. Rumerio, C. West

Boston University, Boston, U.S.A.
A. Akpinar, A. Albert, D. Arcaro, C. Cosby, Z. Demiragli, D. Gastler, C. Richardson, J. Rohlf, K. Salyer, D. Sperka, D. Spitzbart, I. Suarez, S. Yuan, D. Zou

Brown University, Providence, U.S.A.
G. Benelli, B. Burkle, X. Coubez[21], D. Cutts, Y.t. Duh, M. Hadley, U. Heintz, J.M. Hogan[81], K.H.M. Kwok, E. Laird, G. Landsberg, K.T. Lau, J. Lee, M. Narain, S. Sagir[82], R. Syarif, E. Usai, W.Y. Wong, D. Yu, W. Zhang

University of California, Davis, Davis, U.S.A.
R. Band, C. Brainerd, R. Breedon, M. Calderon De La Barca Sanchez, M. Chertok, J. Conway, R. Conway, P.T. Cox, R. Erbacher, C. Flores, G. Funk, F. Jensen, W. Ko[†], O. Kukral, R. Lander, M. Mulhearn, D. Pellett, J. Pilot, M. Shi, D. Taylor, K. Tos, M. Tripathi, Y. Yao, F. Zhang

2020 JINST 15 P10002

University of California, Los Angeles, U.S.A.

M. Bachtis, R. Cousins, A. Dasgupta, A. Florent, D. Hamilton, J. Hauser, M. Ignatenko, T. Lam, N. Mccoll, W.A. Nash, S. Regnard, D. Saltzberg, C. Schnaible, B. Stone, V. Valuev

University of California, Riverside, Riverside, U.S.A.

K. Burt, Y. Chen, R. Clare, J.W. Gary, S.M.A. Ghiasi Shirazi, G. Hanson, G. Karapostoli, O.R. Long, N. Manganelli, M. Olmedo Negrete, M.I. Paneva, W. Si, S. Wimpenny, Y. Zhang

University of California, San Diego, La Jolla, U.S.A.

J.G. Branson, P. Chang, S. Cittolin, S. Cooperstein, N. Deelen, M. Derdzinski, J. Duarte, R. Gerosa, D. Gilbert, B. Hashemi, D. Klein, V. Krutelyov, J. Letts, M. Masciovecchio, S. May, S. Padhi, M. Pieri, V. Sharma, M. Tadel, F. Würthwein, A. Yagil

University of California, Santa Barbara — Department of Physics, Santa Barbara, U.S.A.

N. Amin, C. Campagnari, M. Citron, A. Dorsett, V. Dutta, J. Incandela, B. Marsh, H. Mei, A. Ovcharova, H. Qu, M. Quinnan, J. Richman, U. Sarica, D. Stuart, S. Wang

California Institute of Technology, Pasadena, U.S.A.

D. Anderson, A. Bornheim, O. Cerri, I. Dutta, J.M. Lawhorn, N. Lu, J. Mao, H.B. Newman, T.Q. Nguyen, J. Pata, M. Spiropulu, J.R. Vlimant, S. Xie, Z. Zhang, R.Y. Zhu

Carnegie Mellon University, Pittsburgh, U.S.A.

J. Alison, M.B. Andrews, T. Ferguson, T. Mudholkar, M. Paulini, M. Sun, I. Vorobiev

University of Colorado Boulder, Boulder, U.S.A.

J.P. Cumalat, W.T. Ford, E. MacDonald, T. Mulholland, R. Patel, A. Perloff, K. Stenson, K.A. Ulmer, S.R. Wagner

Cornell University, Ithaca, U.S.A.

J. Alexander, Y. Cheng, J. Chu, D.J. Cranshaw, A. Datta, A. Frankenthal, K. Mcdermott, J. Monroy, J.R. Patterson, D. Quach, A. Ryd, W. Sun, S.M. Tan, Z. Tao, J. Thom, P. Wittich, M. Zientek

Fermi National Accelerator Laboratory, Batavia, U.S.A.

S. Abdullin, M. Albrow, M. Alyari, G. Apollinari, A. Apresyan, A. Apyan, S. Banerjee, L.A.T. Bauerdick, A. Beretvas, D. Berry, J. Berryhill, P.C. Bhat, K. Burkett, J.N. Butler, A. Canepa, G.B. Cerati, H.W.K. Cheung, F. Chlebana, M. Cremonesi, V.D. Elvira, J. Freeman, Z. Gecse, E. Gottschalk, L. Gray, D. Green, S. Grünendahl, O. Gutsche, R.M. Harris, S. Hasegawa, R. Heller, T.C. Herwig, J. Hirschauer, B. Jayatilaka, S. Jindariani, M. Johnson, U. Joshi, P. Klabbers, T. Klijnsma, B. Klima, M.J. Kortelainen, S. Lammel, D. Lincoln, R. Lipton, M. Liu, T. Liu, J. Lykken, K. Maeshima, D. Mason, P. McBride, P. Merkel, S. Mrenna, S. Nahn, V. O'Dell, V. Papadimitriou, K. Pedro, C. Pena[83], O. Prokofyev, F. Ravera, A. Reinsvold Hall, L. Ristori, B. Schneider, E. Sexton-Kennedy, N. Smith, A. Soha, W.J. Spalding, L. Spiegel, S. Stoynev, J. Strait, L. Taylor, S. Tkaczyk, N.V. Tran, L. Uplegger, E.W. Vaandering, M. Wang, H.A. Weber, A. Woodard

University of Florida, Gainesville, U.S.A.

D. Acosta, P. Avery, D. Bourilkov, L. Cadamuro, V. Cherepanov, F. Errico, R.D. Field, D. Guerrero, B.M. Joshi, M. Kim, J. Konigsberg, A. Korytov, K.H. Lo, K. Matchev, N. Menendez, G. Mitselmakher, D. Rosenzweig, K. Shi, J. Wang, S. Wang, X. Zuo

2020 JINST 15 P10002

Florida International University, Miami, U.S.A.

Y.R. Joshi

Florida State University, Tallahassee, U.S.A.

T. Adams, A. Askew, D. Diaz, R. Habibullah, S. Hagopian, V. Hagopian, K.F. Johnson, R. Khurana, T. Kolberg, G. Martinez, H. Prosper, C. Schiber, R. Yohay, J. Zhang

Florida Institute of Technology, Melbourne, U.S.A.

M.M. Baarmand, S. Butalla, T. Elkafrawy[15], M. Hohlmann, D. Noonan, M. Rahmani, M. Saunders, F. Yumiceva

University of Illinois at Chicago (UIC), Chicago, U.S.A.

M.R. Adams, L. Apanasevich, H. Becerril Gonzalez, R. Cavanaugh, X. Chen, S. Dittmer, O. Evdokimov, C.E. Gerber, D.A. Hangal, D.J. Hofman, C. Mills, G. Oh, T. Roy, M.B. Tonjes, N. Varelas, J. Viinikainen, X. Wang, Z. Wu

The University of Iowa, Iowa City, U.S.A.

M. Alhusseini, B. Bilki[64], K. Dilsiz[84], S. Durgut, R.P. Gandrajula, M. Haytmyradov, V. Khristenko, O.K. Köseyan, J.-P. Merlo, A. Mestvirishvili[85], A. Moeller, J. Nachtman, H. Ogul[86], Y. Onel, F. Ozok[87], A. Penzo, C. Snyder, E. Tiras, J. Wetzel, K. Yi[88]

Johns Hopkins University, Baltimore, U.S.A.

O. Amram, B. Blumenfeld, L. Corcodilos, M. Eminizer, A.V. Gritsan, S. Kyriacou, P. Maksimovic, C. Mantilla, J. Roskes, M. Swartz, T.Á. Vámi

The University of Kansas, Lawrence, U.S.A.

C. Baldenegro Barrera, P. Baringer, A. Bean, A. Bylinkin, T. Isidori, S. Khalil, J. King, G. Krintiras, A. Kropivnitskaya, C. Lindsey, N. Minafra, M. Murray, C. Rogan, C. Royon, S. Sanders, E. Schmitz, J.D. Tapia Takaki, Q. Wang, J. Williams, G. Wilson

Kansas State University, Manhattan, U.S.A.

S. Duric, A. Ivanov, K. Kaadze, D. Kim, Y. Maravin, D.R. Mendis, T. Mitchell, A. Modak, A. Mohammadi

Lawrence Livermore National Laboratory, Livermore, U.S.A.

F. Rebassoo, D. Wright

University of Maryland, College Park, U.S.A.

E. Adams, A. Baden, O. Baron, A. Belloni, S.C. Eno, Y. Feng, N.J. Hadley, S. Jabeen, G.Y. Jeng, R.G. Kellogg, T. Koeth, A.C. Mignerey, S. Nabili, M. Seidel, A. Skuja, S.C. Tonwar, L. Wang, K. Wong

Massachusetts Institute of Technology, Cambridge, U.S.A.

D. Abercrombie, B. Allen, R. Bi, S. Brandt, W. Busza, I.A. Cali, Y. Chen, M. D'Alfonso, G. Gomez Ceballos, M. Goncharov, P. Harris, D. Hsu, M. Hu, M. Klute, D. Kovalskyi, J. Krupa, Y.-J. Lee, P.D. Luckey, B. Maier, A.C. Marini, C. Mcginn, C. Mironov, S. Narayanan, X. Niu, C. Paus, D. Rankin, C. Roland, G. Roland, Z. Shi, G.S.F. Stephans, K. Sumorok, K. Tatar, D. Velicanu, J. Wang, T.W. Wang, Z. Wang, B. Wyslouch

2020 JINST 15 P10002

University of Minnesota, Minneapolis, U.S.A.

R.M. Chatterjee, A. Evans, S. Guts[†], P. Hansen, J. Hiltbrand, Sh. Jain, M. Krohn, Y. Kubota, Z. Lesko, J. Mans, M. Revering, R. Rusack, R. Saradhy, N. Schroeder, N. Strobbe, M.A. Wadud

University of Mississippi, Oxford, U.S.A.

J.G. Acosta, S. Oliveros

University of Nebraska-Lincoln, Lincoln, U.S.A.

K. Bloom, S. Chauhan, D.R. Claes, C. Fangmeier, L. Finco, F. Golf, J.R. González Fernández, I. Kravchenko, J.E. Siado, G.R. Snow[†], B. Stieger, W. Tabb

State University of New York at Buffalo, Buffalo, U.S.A.

G. Agarwal, C. Harrington, L. Hay, I. Iashvili, A. Kharchilava, C. McLean, D. Nguyen, A. Parker, J. Pekkanen, S. Rappoccio, B. Roozbahani

Northeastern University, Boston, U.S.A.

G. Alverson, E. Barberis, C. Freer, Y. Haddad, A. Hortiangtham, G. Madigan, B. Marzocchi, D.M. Morse, V. Nguyen, T. Orimoto, L. Skinnari, A. Tishelman-Charny, T. Wamorkar, B. Wang, A. Wisecarver, D. Wood

Northwestern University, Evanston, U.S.A.

S. Bhattacharya, J. Bueghly, Z. Chen, A. Gilbert, T. Gunter, K.A. Hahn, N. Odell, M.H. Schmitt, K. Sung, M. Velasco

University of Notre Dame, Notre Dame, U.S.A.

R. Bucci, N. Dev, R. Goldouzian, M. Hildreth, K. Hurtado Anampa, C. Jessop, D.J. Karmgard, K. Lannon, W. Li, N. Loukas, N. Marinelli, I. Mcalister, F. Meng, K. Mohrman, Y. Musienko[45], R. Ruchti, P. Siddireddy, S. Taroni, M. Wayne, A. Wightman, M. Wolf, L. Zygala

The Ohio State University, Columbus, U.S.A.

J. Alimena, B. Bylsma, B. Cardwell, L.S. Durkin, B. Francis, C. Hill, A. Lefeld, B.L. Winer, B.R. Yates

Princeton University, Princeton, U.S.A.

G. Dezoort, P. Elmer, B. Greenberg, N. Haubrich, S. Higginbotham, A. Kalogeropoulos, G. Kopp, S. Kwan, D. Lange, M.T. Lucchini, J. Luo, D. Marlow, K. Mei, I. Ojalvo, J. Olsen, C. Palmer, P. Piroué, D. Stickland, C. Tully

University of Puerto Rico, Mayaguez, U.S.A.

S. Malik, S. Norberg

Purdue University, West Lafayette, U.S.A.

V.E. Barnes, R. Chawla, S. Das, L. Gutay, M. Jones, A.W. Jung, B. Mahakud, G. Negro, N. Neumeister, C.C. Peng, S. Piperov, H. Qiu, J.F. Schulte, N. Trevisani, F. Wang, R. Xiao, W. Xie

Purdue University Northwest, Hammond, U.S.A.

T. Cheng, J. Dolen, N. Parashar, M. Stojanovic

2020 JINST 15 P10002

Rice University, Houston, U.S.A.

A. Baty, S. Dildick, K.M. Ecklund, S. Freed, F.J.M. Geurts, M. Kilpatrick, A. Kumar, W. Li, B.P. Padley, R. Redjimi, J. Roberts[†], J. Rorie, W. Shi, A.G. Stahl Leiton, A. Zhang

University of Rochester, Rochester, U.S.A.

A. Bodek, P. de Barbaro, R. Demina, J.L. Dulemba, C. Fallon, T. Ferbel, M. Galanti, A. Garcia-Bellido, O. Hindrichs, A. Khukhunaishvili, E. Ranken, R. Taus

Rutgers, The State University of New Jersey, Piscataway, U.S.A.

B. Chiarito, J.P. Chou, A. Gandrakota, Y. Gershtein, E. Halkiadakis, A. Hart, M. Heindl, E. Hughes, S. Kaplan, O. Karacheban[24], I. Laflotte, A. Lath, R. Montalvo, K. Nash, M. Osherson, S. Salur, S. Schnetzer, S. Somalwar, R. Stone, S.A. Thayil, S. Thomas, H. Wang

University of Tennessee, Knoxville, U.S.A.

H. Acharya, A.G. Delannoy, S. Spanier

Texas A&M University, College Station, U.S.A.

O. Bouhali[89], M. Dalchenko, A. Delgado, R. Eusebi, J. Gilmore, T. Huang, T. Kamon[90], H. Kim, S. Luo, S. Malhotra, R. Mueller, D. Overton, L. Perniè, D. Rathjens, A. Safonov, J. Sturdy

Texas Tech University, Lubbock, U.S.A.

N. Akchurin, J. Damgov, V. Hegde, S. Kunori, K. Lamichhane, S.W. Lee, T. Mengke, S. Muthumuni, T. Peltola, S. Undleeb, I. Volobouev, Z. Wang, A. Whitbeck

Vanderbilt University, Nashville, U.S.A.

E. Appelt, S. Greene, A. Gurrola, R. Janjam, W. Johns, C. Maguire, A. Melo, H. Ni, K. Padeken, F. Romeo, P. Sheldon, S. Tuo, J. Velkovska, M. Verweij

University of Virginia, Charlottesville, U.S.A.

L. Ang, M.W. Arenton, B. Cox, G. Cummings, J. Hakala, R. Hirosky, M. Joyce, A. Ledovskoy, C. Neu, B. Tannenwald, Y. Wang, E. Wolfe, F. Xia

Wayne State University, Detroit, U.S.A.

P.E. Karchin, N. Poudyal, P. Thapa

University of Wisconsin — Madison, Madison, WI, U.S.A.

K. Black, T. Bose, J. Buchanan, C. Caillol, S. Dasu, I. De Bruyn, C. Galloni, H. He, M. Herndon, A. Hervé, U. Hussain, A. Lanaro, A. Loeliger, R. Loveless, J. Madhusudanan Sreekala, A. Mallampalli, D. Pinna, T. Ruggles, A. Savin, V. Shang, V. Sharma, W.H. Smith, D. Teague, S. Trembath-reichert, W. Vetens

†: Deceased

1: Also at Vienna University of Technology, Vienna, Austria

2: Also at Department of Basic and Applied Sciences, Faculty of Engineering, Arab Academy for Science, Technology and Maritime Transport, Alexandria, Egypt

3: Also at Université Libre de Bruxelles, Bruxelles, Belgium

4: Also at IRFU, CEA, Université Paris-Saclay, Gif-sur-Yvette, France

5: Also at Universidade Estadual de Campinas, Campinas, Brazil

2020 JINST 15 P10002

6: Also at Federal University of Rio Grande do Sul, Porto Alegre, Brazil
7: Also at UFMS, Nova Andradina, Brazil
8: Also at Universidade Federal de Pelotas, Pelotas, Brazil
9: Also at University of Chinese Academy of Sciences, Beijing, China
10: Also at Institute for Theoretical and Experimental Physics named by A.I. Alikhanov of NRC 'Kurchatov Institute', Moscow, Russia
11: Also at Joint Institute for Nuclear Research, Dubna, Russia
12: Also at Suez University, Suez, Egypt
13: Now at British University in Egypt, Cairo, Egypt
14: Also at Zewail City of Science and Technology, Zewail, Egypt
15: Now at Ain Shams University, Cairo, Egypt
16: Now at Fayoum University, El-Fayoum, Egypt
17: Also at Purdue University, West Lafayette, U.S.A.
18: Also at Université de Haute Alsace, Mulhouse, France
19: Also at Erzincan Binali Yildirim University, Erzincan, Turkey
20: Also at CERN, European Organization for Nuclear Research, Geneva, Switzerland
21: Also at RWTH Aachen University, III. Physikalisches Institut A, Aachen, Germany
22: Also at University of Hamburg, Hamburg, Germany
23: Also at Department of Physics, Isfahan University of Technology, Isfahan, Iran, Isfahan, Iran
24: Also at Brandenburg University of Technology, Cottbus, Germany
25: Also at Skobeltsyn Institute of Nuclear Physics, Lomonosov Moscow State University, Moscow, Russia
26: Also at Institute of Physics, University of Debrecen, Debrecen, Hungary, Debrecen, Hungary
27: Also at Physics Department, Faculty of Science, Assiut University, Assiut, Egypt
28: Also at MTA-ELTE Lendület CMS Particle and Nuclear Physics Group, Eötvös Loránd University, Budapest, Hungary, Budapest, Hungary
29: Also at Institute of Nuclear Research ATOMKI, Debrecen, Hungary
30: Also at IIT Bhubaneswar, Bhubaneswar, India, Bhubaneswar, India
31: Also at Institute of Physics, Bhubaneswar, India
32: Also at G.H.G. Khalsa College, Punjab, India
33: Also at Shoolini University, Solan, India
34: Also at University of Hyderabad, Hyderabad, India
35: Also at University of Visva-Bharati, Santiniketan, India
36: Also at Indian Institute of Technology (IIT), Mumbai, India
37: Also at Deutsches Elektronen-Synchrotron, Hamburg, Germany
38: Also at Department of Physics, University of Science and Technology of Mazandaran, Behshahr, Iran
39: Now at INFN Sezione di Bari[a], Università di Bari[b], Politecnico di Bari[c], Bari, Italy
40: Also at Italian National Agency for New Technologies, Energy and Sustainable Economic Development, Bologna, Italy
41: Also at Centro Siciliano di Fisica Nucleare e di Struttura Della Materia, Catania, Italy
42: Also at Riga Technical University, Riga, Latvia, Riga, Latvia
43: Also at Consejo Nacional de Ciencia y Tecnología, Mexico City, Mexico
44: Also at Warsaw University of Technology, Institute of Electronic Systems, Warsaw, Poland
45: Also at Institute for Nuclear Research, Moscow, Russia
46: Now at National Research Nuclear University 'Moscow Engineering Physics Institute' (MEPhI), Moscow, Russia
47: Also at St. Petersburg State Polytechnical University, St. Petersburg, Russia
48: Also at University of Florida, Gainesville, U.S.A.
49: Also at Imperial College, London, United Kingdom
50: Also at P.N. Lebedev Physical Institute, Moscow, Russia

2020 JINST 15 P10002

51: Also at INFN Sezione di Padova[a], Università di Padova[b], Padova, Italy, Università di Trento[c], Trento, Italy, Padova, Italy
52: Also at Budker Institute of Nuclear Physics, Novosibirsk, Russia
53: Also at Faculty of Physics, University of Belgrade, Belgrade, Serbia
54: Also at Università degli Studi di Siena, Siena, Italy
55: Also at Trincomalee Campus, Eastern University, Sri Lanka, Nilaveli, Sri Lanka
56: Also at INFN Sezione di Pavia[a], Università di Pavia[b], Pavia, Italy, Pavia, Italy
57: Also at National and Kapodistrian University of Athens, Athens, Greece
58: Also at Universität Zürich, Zurich, Switzerland
59: Also at Stefan Meyer Institute for Subatomic Physics, Vienna, Austria, Vienna, Austria
60: Also at Laboratoire d'Annecy-le-Vieux de Physique des Particules, IN2P3-CNRS, Annecy-le-Vieux, France
61: Also at Şirnak University, Sirnak, Turkey
62: Also at Department of Physics, Tsinghua University, Beijing, China, Beijing, China
63: Also at Near East University, Research Center of Experimental Health Science, Nicosia, Turkey
64: Also at Beykent University, Istanbul, Turkey, Istanbul, Turkey
65: Also at Istanbul Aydin University, Application and Research Center for Advanced Studies (App. & Res. Cent. for Advanced Studies), Istanbul, Turkey
66: Also at Mersin University, Mersin, Turkey
67: Also at Piri Reis University, Istanbul, Turkey
68: Also at Adiyaman University, Adiyaman, Turkey
69: Also at Ozyegin University, Istanbul, Turkey
70: Also at Izmir Institute of Technology, Izmir, Turkey
71: Also at Necmettin Erbakan University, Konya, Turkey
72: Also at Bozok Universitetesi Rektörlügü, Yozgat, Turkey
73: Also at Marmara University, Istanbul, Turkey
74: Also at Milli Savunma University, Istanbul, Turkey
75: Also at Kafkas University, Kars, Turkey
76: Also at Istanbul Bilgi University, Istanbul, Turkey
77: Also at Hacettepe University, Ankara, Turkey
78: Also at School of Physics and Astronomy, University of Southampton, Southampton, United Kingdom
79: Also at IPPP Durham University, Durham, United Kingdom
80: Also at Monash University, Faculty of Science, Clayton, Australia
81: Also at Bethel University, St. Paul, Minneapolis, U.S.A., St. Paul, U.S.A.
82: Also at Karamanoğlu Mehmetbey University, Karaman, Turkey
83: Also at California Institute of Technology, Pasadena, U.S.A.
84: Also at Bingol University, Bingol, Turkey
85: Also at Georgian Technical University, Tbilisi, Georgia
86: Also at Sinop University, Sinop, Turkey
87: Also at Mimar Sinan University, Istanbul, Istanbul, Turkey
88: Also at Nanjing Normal University Department of Physics, Nanjing, China
89: Also at Texas A&M University at Qatar, Doha, Qatar
90: Also at Kyungpook National University, Daegu, Korea, Daegu, Korea

2020 JINST 15 P10002